Tetranuclear Manganese-Oxo Aggregates Relevant to the Photosynthetic Water Oxidation Center. Crystal Structure, Spectroscopic Properties and Reactivity of Adamantane-Shaped $[Mn_4O_6(bpea)_4]^{4+}$ and the Reduced Mixed-Valence Analog $[Mn_4O_6(bpea)_4]^{3+}$

Christopher E. Dubé, David W. Wright,† Samudranil Pal,‡ Peter J. Bonitatebus, Jr., and William H. Armstrong*

Contribution from the Department of Chemistry, Eugene F. Merkert Chemistry Center, Boston College, Chestnut Hill, Massachusetts 02167-3860

Received October 22, 1997

Abstract: The tetranuclear Mn^{IV} adamantane-like complex $[Mn_4O_6(bpea)_4](ClO_4)_4$(**1**$(ClO_4)_4$) was isolated from a comproportionation reaction of $Mn(ClO_4)_2 \cdot 6H_2O$ and [*n*-Bu_4N][MnO_4] with the ligand *N*,*N*-bis(2-pyridylmethyl)ethylamine (bpea) in acetonitrile. Characterization by X-ray crystallography reveals that the $[Mn_4O_6(bpea)_4]^{4+}$ cation approaches S_4 point symmetry. There are three distinct types of Mn−N bonds and two types of bridging oxo ligands in **1**. ^{1}H NMR protonation studies of **1** in acetonitrile reveal that each type of oxo bridge renders a different protonation isomer and that the isomers are readily distinguished by their differences in solution structural symmetry and oxo bridge acidity. In addition, pH-dependent aqueous electrochemical studies show that the proton-coupled electron-transfer behavior of **1** is significant because it is the first example of a Mn-oxo aggregate exhibiting a $e^-/2H^+$ stoichiometry and because it displays pH-dependent e^-/H^+ stoichiometry. Remarkably, reaction of **1**$(BF_4)_4$ with the tridentate nitrogen donor ligand 1,4,7-trimethyl-1,4,7-triazacyclononane (Me_3tacn) in acetonitrile affords the one-electron reduced complex $[Mn_4O_6(bpea)_4](BF_4)_3$ (**2**$(BF_4)_3$), rather than the anticipated ligand substituted product. Like **1**, the $[Mn_4O_6(bpea)_4]^{3+}$ cation also contains the adamantane skeleton. The $(Mn^{III})(Mn^{IV})_3$ cluster of **2** contains a crystallographically distinguishable Mn^{III} ion, as noted by elongation along the N_{alkyl}-Mn−O_{oxo} axis. The ^{1}H NMR solution spectrum of **2** is consistent with a valence-delocalized $(Mn^{III})(Mn^{IV})_3$ cluster, indicating fast intramolecular electron transfer on the NMR time scale, and redox titration of **1** to **2** indicates slow intermolecular electron transfer on the same time scale. Solution magnetic susceptibility measurements in acetonitrile show that conversion of **1**$(ClO_4)_4$ to **2**$(ClO_4)_3$ is attendant with a change from net ferromagnetic coupling to overall moderate antiferromagnetic coupling within the manganese-oxo core. Isolation of the $\{Mn_4O_6\}$ core in the $(IV)_4$ *and* $(III)(IV)_3$ oxidation states is facilitated by the relatively weak donor nature of the bpea ligand, in marked contrast to the strongly basic donor ligands 1,4,7-triazacyclononane (tacn) and 1,1,1-tris(aminomethyl)ethane (tame), which stabilize the higher oxidation state of the $\{Mn_4O_6\}$ cluster, making the one-electron reduced form less accessible. The novel protonation and electrochemical properties of **1** are discussed in the context of the Kok cycle of photosynthetic water oxidation.

Introduction

The oxygen-evolving complex (OEC) of Photosystem II (PSII) contains the unique manganese-oxo aggregate responsible for catalysis of the oxidation of water to dioxygen.[1−19] Despite the host of biophysical methods used to examine the OEC, an accurate model for the active site aggregate has not been forthcoming. Nevertheless, extended X-ray absorption fine structure (EXAFS) studies reveal at least two 2.7 Å Mn···Mn

† Present address: Duquesne University, Pittsburgh, PA, 15282.

‡ Present address: University of Hyderabad, Hyderabad 500 046, India.

(1) Debus, R. J. *Biochim. Biophys. Acta* **1992**, *1102*, 269−352.

(2) Randall, D. W.; Sturgeon, B. E.; Ball, J. A.; Lorigan, G. A.; Chan, M. K.; Klein, M. P.; Armstrong, W. H.; Britt, R. D. *J. Am. Chem. Soc.* **1995**, *117*, 11780−11789.

(3) Britt, R. D. In *Oxygenic Photosynthesis: The Light Reactions*; Ort, D. R., Yocum, C. F., Eds.; Kluwer Academic Publishers: Dordrecht, Netherlands, 1996; pp 137−164.

(4) Penner-Hahn, J. E.; Fronko, R. M.; Pecoraro, V. L.; Yocum, C. F.; Betts, S. D.; Bowlby, N. R. *J. Am. Chem. Soc.* **1990**, *112*, 2549−2557.

(5) Kirby, J. A.; Robertson, A. S.; Smith, J. P.; Thompson, A. C.; Cooper, S. R.; Klein, M. P. *J. Am. Chem. Soc.* **1981**, *103*, 5529−5537.

(6) MacLachlan, D. J.; Hallahan, B. J.; Ruffle, S. V.; Nugent, J. H. A.; Evans, M. C. W.; Strange, R. W.; Hasnain, S. S. *Biochem. J.* **1992**, *285*, 569−576.

(7) DeRose, V. J.; Mukerji, I.; Latimer, M. J.; Yachandra, V. K.; Sauer, K.; Klein, M. P. *J. Am. Chem. Soc.* **1994**, *116*, 5239−5249.

(8) Dismukes, G. C.; Siderer, Y. *FEBS Lett.* **1980**, 78−80.

(9) Dismukes, G. C.; Siderer, Y. *Proc. Natl. Acad. Sci. U.S.A.* **1981**, *78*, 274−278.

(10) Casey, J. L.; Sauer, K. *Biochim. Biophys. Acta* **1984**, *767*, 21−28.

(11) Zimmermann, J. L.; Rutherford, A. W. *Biochim. Biophys. Acta* **1984**, 160−167.

(12) Kim, D. H.; Britt, R. D.; Klein, M. P.; Sauer, K. *J. Am. Chem. Soc.* **1990**, *112*, 9389−9391.

(13) Brudvig, G. W. In *Advanced EPR: Applications in Biology and Biochemistry*; Hoff, A. J., Ed.; Elsevier: Amsterdam, 1990; pp 839−863.

(14) Kusunoki, M. *Chem. Phys. Lett.* **1992**, *197*, 108−116.

(15) Zheng, M.; Dismukes, G. C. In *Research in Photosynthesis*; Murata, N., Ed.; Kluwer Academic Publishers: Dordrecht, Netherlands, 1992; Vol. II, pp 305−308.

S0002-7863(97)03668-8 CCC: $15.00
Published on Web 04/02/1998

vectors[4−7,19] as well as a longer 3.3 Å Mn···Mn (or Mn···Ca) vector,[4,6,7] indicating that the four Mn atoms are likely arranged in a tightly bridged cluster. In addition, the PSII S_2 oxidation state shows two characteristic electron paramagnetic resonance (EPR) signals associated with the manganese center: a 19−21 line signal centered at $g = 2$[8,9] and a broader signal centered at $g = 4.1$,[10,11] which in oriented PSII samples has at least 16 hyperfine lines.[12] Interpretations of the S_2 state EPR behavior suggest a model in which all manganese atoms are appreciably coupled to the multiline spin.[13−17] Recently, a ^{55}Mn electron spin echo−external nuclear double resonance (ESE−ENDOR) study of the S_2 state of PSII concluded that a spin-coupled tetranuclear model for the Mn cluster provides the best parameter set for simulation of both EPR and ^{55}Mn ENDOR spectra.[2] Although the precise structure of the cluster remains an issue of intense interest, it is generally accepted that the manganese aggregate at the heart of the water oxidase active site consists of four manganese atoms.

Some insight into the structure and mechanism of action of the OEC has been achieved through synthesis, characterization, and reactivity studies of high valent tetranuclear manganese-oxo aggregates such as the adamantane-shaped $\{Mn_4(\mu\text{-}O)_6\}^{4+}$,[20−22] $\{Mn_4(\mu\text{-}O)_5(OH)\}^{5+}$,[22] and $\{Mn_4(\mu\text{-}O)_4(OH)_2\}^{6+}$,[23] the cubane-like $\{Mn_4(\mu_3\text{-}O)_3(\mu_3\text{-}X)\}^{4+}$ [24−26] and $\{Mn_4(\mu_3\text{-}O)_4\}^{6+}$,[27] the "butterfly" $\{Mn_4(\mu_3\text{-}O)_2(\mu\text{-}OAc)_7\}^{+}$,[28,29] the dimer-of-dimers $\{Mn_2(\mu\text{-}O)_2(\mu\text{-}OR)\}_2^{4+}$,[30] and the "linear" $\{Mn_4(\mu\text{-}O)_6\}^{4+}$ and $\{Mn_4(\mu\text{-}O)_6\}^{3+}$ cores.[31−33] The cubane and adamantane cores are featured prominently in the mechanism proposed by Brudvig and Crabtree,[34,35] and the "butterfly" and cubane cores serve as the active site intermediates in the double-pivot mechanism proposed by Christou.[36] Although none of the above complexes has been shown to exhibit water oxidation, reactivity believed relevant to the water oxidase cycle, such as protonation and reversible electron-transfer, has been described. Recently, we have shown that the adamantane-like $[Mn_4O_6(tacn)_4]^{4+}$ core can undergo successive reversible protonation of the oxo-bridges to yield $[Mn_4O_4(OH)_2(tacn)_4]^{6+}$.[23] Sequential deprotonation of $[Mn_4O_4(OH)_2(tacn)_4]^{6+}$ results in increasingly overall ferromagnetic coupling within the complex similar to the trend observed between the S_1 and S_2 states of the OEC of PSII.[38,39] The $[Mn_4O_6(tacn)_4]^{4+}$ complex also demonstrates two quasi-reversible redox couples in CH_3CN.[40] Such processes have important biological implications. Both electron- and proton-transfer chemistry are critical components of the Kok cycle[41] as well as various proposed mechanisms for water oxidation that emphasize the deprotonation of H_2O to form terminal or bridging O^{2-} or OH^- ligands at the active site. For these reasons, an understanding of the factors which influence the protonation and redox behavior of tetranuclear manganese-oxo clusters is essential in order to activate a core toward substrate oxidation.

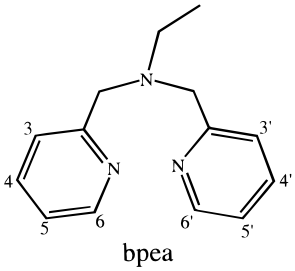

bpea

Figure 1. The bpea ligand with numbering scheme used in the text.

In an ongoing effort to understand the aggregation and physical properties of manganese-oxo clusters, we have synthesized a number of di- and trinuclear manganese-oxo aggregates using the ligand bpea and its analogs.[42−45] In contrast to the tacn and tame ligands, bpea (Figure 1) is capable of

(16) Bonvoisin, J.; Blondin, G.; Girerd, J.-J.; Zimmermann, J.-L. *Biophys. J.* **1992**, *61*, 1076−1086.
(17) Belinski, M. I. *Chem. Phys.* **1994**, *179*, 1−22.
(18) Yachandra, V. K.; DeRose, V. J.; Latimer, M. J.; Mukerji, I.; Sauer, K.; Klein, M. P. *Science* **1993**, *260*, 675−679.
(19) Yachandra, V. K.; Sauer, K.; Klein, M. P. *Chem. Rev.* **1996**, *96*, 2927−2950.
(20) Wieghardt, K.; Bossek, U.; Gebert, W. *Angew. Chem., Int. Ed. Engl.* **1983**, *22*, 328−329.
(21) Wieghardt, K.; Bossek, U.; Nuber, B.; Weiss, J.; Bonvoisin, J.; Corbella, M.; Vitols, S. E.; Girerd, J.-J. *J. Am. Chem. Soc.* **1988**, *110*, 7398−7411.
(22) Hagen, K. S.; Westmoreland, T. D.; Scott, M. J.; Armstrong, W. H. *J. Am. Chem. Soc.* **1989**, *111*, 1907−1909.
(23) Dubé, C. E.; Wright, D. W.; Armstrong, W. H. *J. Am. Chem. Soc.* **1996**, *118*, 10910−10911.
(24) Hendrickson, D. N.; Christou, G.; Schmitt, E. A.; Libby, E.; Baskin, J. S.; Wang, S.; Tsai, H.; Vincent, J. B.; Boyd, P. D. W.; Haffman, J. C.; Folting, K.; Li, Q.; Streib, W. E. *J. Am. Chem. Soc.* **1992**, *114*, 2455−2471.
(25) Wemple, M. W.; Tsai, H.-L.; Folting, K.; Hendrickson, D. N.; Christou, G. *Inorg. Chem.* **1993**, *32*, 2025−2031.
(26) Wemple, M. W.; Adams, D. M.; Folting, K.; Hendrickson, D. N.; Christou, G. *J. Am. Chem. Soc.* **1995**, *117*, 7275−7276.
(27) Ruettinger, W. F.; Campana, C.; Dismukes, G. C. *J. Am. Chem. Soc.* **1997**, *119*, 6670−6671.
(28) Vincent, J. B.; Christmas, C.; Chang, H. R.; Li, Q.; Boyd, P. D. W.; Huffman, J. C.; Hendrickson, D. N.; Christou, G. *J. Am. Chem. Soc.* **1989**, *111*, 2086−2097.
(29) Libby, E.; McCusker, J. K.; Schmitt, E. A.; Folting, K.; Hendrickson, D. N.; Christou, G. *Inorg. Chem.* **1991**, *30*, 3486-3495.
(30) Chan, M. K.; Armstrong, W. H. *J. Am. Chem. Soc.* **1991**, *113*, 5055−5057.
(31) Philouze, C.; Blondin, G.; Menage, S.; Auger, N.; Girerd, J.-J.; Vigner, D.; Lance, M.; Nierlich, M. *Angew. Chem., Int. Ed. Engl.* **1992**, *31*, 1629−1631.
(32) Philouze, C.; Blondin, G.; Girerd, J.-J.; Guilhem, J. *J. Am. Chem. Soc.* **1994**, *116*, 8557−8565.
(33) Blondin, G.; Davydov, R.; Philouze, C.; Charlot, M.-F.; Styring, S.; Åkermark, B.; Girerd, J.-J.; Boussac, A. *J. Chem. Soc., Dalton Trans.* **1997**, 4069−4074.
(34) Brudvig, G. W.; Crabtree, R. H. *Proc. Natl. Acad. Sci. U.S.A.* **1986**, *83*, 4586−4588.
(35) Brudvig, G. W.; De Paula, J. C. In *Progress in Photosynthesis Research*; Biggins, J., Ed.; Martinas Nijhoff: The Hague, 1987; Vol. 1, pp 491−498.
(36) Christou, G.; Vincent, J. B. *Biochim. Biophys. Acta* **1987**, *895*, 259−274.
(37) Abbreviations used: bpea, *N*,*N*-bis(2-pyridylmethyl)ethylamine; bpma, *N*,*N*-bis(2-pyridylmethyl)methylamine; 4,4′-Me$_2$bpma, *N*,*N*-bis(4-methyl-2-pyridylmethyl)methylamine; 5,5′-Me$_2$bpma, *N*,*N*-bis(5-methyl-2-pyridylmethyl)methylamine; tacn, 1,4,7-triazacyclononane; tame, 1,1,1-tris(aminomethyl)ethane; TBAP, tetrabutylammonium perchlorate; Me$_3$tacn, 1,4,7-trimethyl-1,4,7-triazacyclononane; tmpa, tris(2-methylpyridyl)amine; bispicen, *N*,*N*′-bis(2-methylpyridyl)-1,2-ethanediamine; bispictn, *N*,*N*′- bis-(2-methylpyridyl)-1,3-propanediamine; Fe(Cp*)$_2$, bis(pentamethylcyclopentadienyl)iron.
(38) Baumgarten, M.; Philo, J. S.; Dismukes, G. C. *Biochemistry* **1990**, *29*, 10814−10822.
(39) Sivaraja, M.; Philo, J. S.; Lary, J.; Dismukes, G. C. *J. Am. Chem. Soc.* **1989**, *111*, 3221−3225.
(40) The (IV,IV,IV,IV)/(V,IV,IV,IV) and (IV,IV,IV,IV)/(III,IV,IV,IV) couples of $[Mn_4O_6(tacn)_4](ClO_4)_4$ (1.32 V and −0.68 V versus SCE, respectively) and $[Mn_4O_6(tame)_4](CF_3SO_3)_4$ (1.20 V and −0.60 V versus SCE, respectively) have been observed in acetonitrile (Wright, D. W.; Dubé, C. E.; Hagen, S. K.; Westmoreland, T. D.; Scott, M. J.; Armstrong, W. H. Manuscript in preparation).
(41) Kok, B.; Forbrush, B.; McGloin, M. *Photochem. Photobiol.* **1970**, *11*, 457−475.
(42) Mok, H. J.; Davis, J. A.; Pal, S.; Mandal, S. K.; Armstrong, W. H. *Inorg. Chim. Acta* **1997**, *263*, 385−394.
(43) Mandal, S. K.; Armstrong, W. H. *Inorg. Chim. Acta* **1995**, *229*, 261−270.
(44) Pal, S.; Olmstead, M. M.; Armstrong, W. H. *Inorg. Chem.* **1995**, *34*, 4708−4715.
(45) Pal, S.; Chan, M.; Armstrong, W. H. *J. Am. Chem. Soc.* **1992**, *114*, 6398−6406.

adopting both meridional and facial coordination to manganese atoms. Also, it is expected that the considerable differences in basicity between bpea and tacn or tame will significantly alter the ligand substitution, redox, and protonation behavior of manganese-oxo complexes of bpea relative to their tacn or tame analogs. Additionally, the steric and electronic properties of bpea are readily altered via synthetic means. With the bpea ligand, the tetranuclear complex $[Mn_4O_6(bpea)_4]^{4+}$ was envisioned as a more reactive adamantane-shaped manganese-oxo aggregate. Herein, the synthesis, X-ray structure, and spectroscopic properties of the adamantane-like cluster $[Mn_4O_6(bpea)_4]^{4+}$ (**1**) and the reduced mixed-valence analog $[Mn_4O_6(bpea)_4]^{3+}$ (**2**) are reported. We also present the novel protonation and electrochemical properties of **1** and discuss these in the context of the proton and electron-transfer chemistry of the Kok cycle of water oxidation.

Experimental Section

Materials. The ligands bpea and bpma were prepared as described elsewhere.[42−44] Synthesis of the methyl-substituted analogs of bpma, 4,4′-Me_2bpma and 5,5′-Me_2bpma was based on literature procedures[46,47] modified by K. D. Karlin (personal communication) and is described elsewhere.[48] The complexes $[n\text{-}Bu_4N][MnO_4]$,[49] $[Mn_4O_6(tacn)_4](ClO_4)_4$,[22] and the sodium salt of $[[3,5\text{-}(CF_3)_2C_6H_3]_4B]^-$ ($NaBAr'_4$)[50] were synthesized as reported. Acetonitrile used for electrochemical and UV−vis experiments was distilled from CaH_2 and stored under argon over 3 Å molecular sieves for at least one week prior to use. Deuterated acetonitrile (Cambridge Isotope Laboratories, Inc.) was dried twice under argon over activated 3 Å molecular sieves. $Fe(Cp^*)_2$ (Strem Chemicals, Inc.), Me_3tacn (Aldrich), and electrochemical grade tetra-*n*-butylammonium perchlorate (TBAP) (Fluka) were used as received. Deionized water (Millipore Milli-Q_{PLUS}) was used for all experiments performed in aqueous media. Phosphate buffer solutions were prepared by standard methods. $H_2{}^{18}O$ (97 atom % ^{18}O) was from Isotech, Inc., and Paratone-N oil was from Exxon. All chemicals used in this work were of reagent grade.

Physical Methods. Electronic spectra were collected using a Cary 1E UV−vis spectrophotometer. ^1H NMR data were collected on a Varian Unity 300 MHz NMR spectrometer with a 100 kHz sweep width. All ^1H NMR spectra were background corrected using a first-order correction function. Values for chemical shifts (ppm) are the observed shifts referenced to the residual protic solvent peak (CHD_2CN, 1.94 ppm). IR spectra were recorded using a Nicolet 5DX FT-IR spectrometer using either KBr disks or acetonitrile solutions. Solid-state magnetic susceptibility measurements were performed on a Quantum Design SQUID magnetometer in the temperature range 6−230 K. All data were corrected for the susceptibility of the empty sample container. Solution magnetic susceptibility characteristics were determined by the NMR method[51−53] at 295 K. Molar paramagnetic susceptibilities were obtained by using diamagnetic corrections ($\chi_d = -826 \times 10^{-6}$, -794×10^{-6}, and -892×10^{-6} cgs/mol for $\mathbf{1}(ClO_4)_4$, $\mathbf{2}(ClO_4)_3$, and $[Mn_4O_5(OH)(bpea)_4](CF_3SO_3)_5$, respectively) calculated from Pascal's constants.[54] Elemental analyses were obtained from Desert Analytics, Tucson, AZ, or Robertson Laboratory, Madison, NJ. Electrospray mass spectrometry (ES−MS) (typically 2×10^{-4} M in acetonitrile, 3.5 kV nebulizer voltage) was performed at the University of Illinois Mass Spectrometry Laboratory.

Electrochemistry. An EG&G PAR model 264A Polarographic Analyzer/Stripping Voltameter or a BAS-100B Electrochemical Analyzer was used for electrochemical experiments. A platinum disk working electrode and a platinum wire auxiliary electrode were used to collect cyclic voltammograms. A saturated sodium calomel electrode (SSCE) and a $Ag/AgClO_4$ electrode were used for reference electrodes in aqueous and acetonitrile solutions, respectively. Phosphate buffer solutions (0.1 M) used for pH-dependent electrochemistry studies were adjusted to the desired pH with NaOH (0.1 M) or HCl (0.1 M) after the addition of complex. The ionic strength was adjusted with 0.1 M NaCl. Electrochemical measurements in acetonitrile used 0.1 M TBAP as supporting electrolyte. Under these conditions the $E_{1/2}$ of the Fc/Fc^+ couple was 0.090 V. Potentials are reported versus SCE by correcting $E_{1/2}$ data to the Fc/Fc^+ couple in acetonitrile versus an SCE reference (0.38 V).[55] Coulometric experiments in acetonitrile employed a platinum wire-mesh working electrode, a porous Vycor frit-isolated Pt coil counter electrode, and a $Ag/AgClO_4$ reference electrode. All electrochemical measurements were performed under a dry and purified dinitrogen atmosphere. The potentials reported in this work are uncorrected for a junction contribution.

Synthesis of Complexes. (a) $[Mn_4O_6(bpea)_4](ClO_4)_4$(1($ClO_4)_4$). $Mn(ClO_4)_2\cdot 6H_2O$ (272 mg, 0.75 mmol) was added to an acetonitrile solution (20 mL) of bpea (284 mg, 1.25 mmol). To this nearly colorless mixture, an acetonitrile solution (5 mL) of $[n\text{-}Bu_4N][MnO_4]$ (181 mg, 0.5 mmol) was added dropwise over a period of 10−15 min. After the mixture was stirred at room temperature for 1 h, the deep brown solution was evaporated to dryness. Uncomplexed ligand and manganese-containing products other than $\mathbf{1}(ClO_4)_4$[56] were extracted by slurrying the resulting solid in 30 mL of MeOH at 50 °C for 1 h. The suspension was filtered and the dark residue was extracted with 15 mL of acetonitrile. To the filtered green acetonitrile solution, 10 mL of toluene was added, and the solution was allowed to evaporate slowly under ambient conditions. The dark crystalline product was collected by filtration. A typical yield of $\mathbf{1}(ClO_4)_4$ by this method is 150 mg (30.4%). Anal. Calcd for $Mn_4Cl_4O_{22}C_{56}H_{68}N_{12}$: Mn, 13.54; C, 41.45; H, 4.22; N, 10.36. Found: Mn, 13.40; C, 41.12; H, 4.03; N, 9.95. Selected IR bands[57] (cm^{-1}) 1607 (s), 1574 (m), 1484 (s), 1436 (s), 1393 (m), 1281 (s), 1232 (w), 1161 (m), 1094 (vs), 1056 (sh), 1029 (s), 994 (w), 918 (w) 862 (w), 769 (s), 710 (s), 622 (s), 508 (w), 470 (w), 438 (w). Electronic spectral data in CH_3CN solution (λ_{max}, nm; ϵ, M^{-1} cm^{-1}): 1014 (270), 580 (2070), 355 (sh).

Anion derivatives of $\mathbf{1}(ClO_4)_4$ using Br^-, BF_4^-, $CF_3SO_3^-$, PF_6^-, SbF_6^-, SCN^-, and $BAr'_4{}^-$ were prepared to vary the solubility properties of **1**, but otherwise exhibited cation IR, MS, electronic, and ^1H NMR spectral characteristics similar to those of the $\mathbf{1}(ClO_4)_4$ cation. A tabulation of metathesis yields, elemental analyses, MS, and IR spectral data for all anion derivatives of $\mathbf{1}(ClO_4)_4$ is given in Supporting Information Table S1.

(b) $[Mn_4O_6(bpea)_4]Br_4$(1Br_4). An acetonitrile solution (1.0 mL) of $[n\text{-}Bu_4N][Br]$ (0.271 g, 0.84 mmol) was added to a green acetonitrile solution (6 mL) of $\mathbf{1}(ClO_4)_4$ (200 mg, 0.12 mmol) and allowed to evaporate to 2 mL under ambient conditions over a 24 h period. The resulting dark crystalline material was filtered, washed with a small amount of ice-cold acetonitrile, and dried under vacuum.

(c) $[Mn_4O_6(bpea)_4]X_4$(1X_4). Complexes of $\mathbf{1}X_4$ ($X = BF_4^-$, $CF_3SO_3^-$, PF_6^-, SCN^-, and $BAr'_4{}^-$) were synthesized by adding seven equivalents of the sodium or potassium salt of the desired anion as a concentrated aqueous solution to an aqueous solution of $\mathbf{1}Br_4$. For $X = PF_6^-$ and $BAr'_4{}^-$, the metathesis product precipitated immediately from solution following addition of the desired anion and was washed with ice-cold water and dried under vacuum over P_2O_5. For $X = BF_4^-$, SCN^-, and $CF_3SO_3^-$, the metathesis solution was allowed to evaporate

(46) Hardegger, E.; Nikles, E. *Helv. Chim. Acta* **1957**, *40*, 2428−2433.
(47) Baker, W.; Buggle, K. M.; McOmie, J. F. W.; Watkins, D. A. M. *J. Chem. Soc.* **1958**, 3594−3603.
(48) Wright, D. W.; Mok, H. J.; Armstrong, W. H. *Inorg. Chem.* Submitted for publication.
(49) Sala, T.; Sargent, M. V. *J. Chem. Soc. Chem. Commun.* **1978**, 253−254.
(50) Bahr, S. R.; Boudjouk, P. *J. Org. Chem.* **1992**, *57*, 5545−5547.
(51) Evans, D. J. *J. Chem. Soc.* **1959**, 2003−2005.
(52) Dickinson, W. C. *Phys. Rev.* **1951**, *81*, 717−731.
(53) Live, D. H.; Chan, S. I. *Anal. Chem.* **1970**, *42*, 791−792.
(54) Mulay, L. N. In *Theory and Applications of Molecular Paramagnetism*; Boudreaux, E. A., Mulay, L. N., Ed.; Wiley: New York, 1976.
(55) Connelly, N. G.; Geiger, W. E. *Chem. Rev.* **1996**, *96*, 877−910.
(56) Examination of the crude reaction by ^1H NMR shows that $\mathbf{1}(ClO_4)_4$ and $[Mn_3O_4(OH)(bpea)_3](ClO_4)_3$ (Pal, S.; Chan, M.; Armstrong, W. H. *J. Am. Chem. Soc.* **1992**, *114*, 6398−6406) are the only *identifiable* high oxidation state products obtained. EPR experiments performed at 77 K do, however, show a six-line signal centered at $g = 2.0$ indicating the presence of an unidentified Mn(II) contaminant. The manganese contaminants were extracted from the crude reaction product as described.
(57) Symbols: vs, very strong; s, strong; m, medium; w, weak; sh, shoulder.

Table 1. Crystallographic Data for $[Mn_4O_6(bpea)_4](ClO_4)_4 \cdot 5CH_3CN$ and $[Mn_4O_6(bpea)_4](BF_4)_3 \cdot 5CH_3CN$

	1$(ClO_4)_4 \cdot 5CH_3CN$	**2**$(BF_4)_3 \cdot 5CH_3CN$
empirical formula	$C_{66}H_{83}Cl_4Mn_4N_{17}O_{22}$	$C_{66}H_{83}B_3F_{12}Mn_4N_{17}O_6$
formula weight	1827.92	1671.53
crystal system	Triclinic	Triclinic
space group	$P\bar{1}$	$P\bar{1}$
a, Å	13.2629(2)	13.8932(2)
b, Å	16.0216(2)	15.8395(3)
c, Å	20.6029(3)	19.3507(5)
α, deg	87.626(1)	81.389(1)
β, deg	84.723(1)	83.607(1)
γ, deg	67.17(1)	66.656(1)
volume, Å^3	4017.7(1)	3832.1(1)
Z	2	2
ρ(calc), g/cm^3	1.497	1.449
2θ range for data collection	3.38−56.58	4.26−56.58
reflections collected	24 783	10 646
independent reflections	17 410 [R(int) = 0.0357]	10 613 [R(int) = 0.0490]
data/restraints/parameters	17 402/0/1046	10597/0/973
goodness-of-fit of F^2	1.094	1.190
final R indices [I > 2σ(I)]	$R_1 = 0.0821$, $wR_2 = 0.2135$	$R_1 = 0.1013$, $wR_2 = 0.2197$

(final volume about 2 mL for a 200 mg sample of **1**Br_4) under ambient conditions and the resulting dark crystalline material was filtered, washed with a small amount of ice-cold water, and dried under vacuum over P_2O_5.

(d) $[Mn_4{}^{18}O_6(bpea)_4](ClO_4)_4$. Substitution of the bridging oxo ligands of **1**Br_4 with ^{18}O was performed using an aqueous solution (300 μL, 97 atom % ^{18}O) of **1**Br_4 (45 mg, 29 μmol) stored under dry Ar. The complex exhibited slight degradation in water over the course of the 3 month experiment as evidenced by precipitation of a brown flocculant material, presumably MnO_2. The course of the bridge substitution reaction was monitored with ES−MS using the $[M\text{-}ClO_4]^+$ ion, and IR analysis using a Mn−O−Mn stretch (*vide infra*) of the perchlorate salt of **1**, which was precipitated by addition of a slight excess of $NaClO_4$ to a filtered aliquot of the **1**Br_4 solution. An ^{18}O enrichment of 90% (based on MS) was achieved after 3 months. The yield was 30 mg (67%).

(e) $[Mn_4O_6(bpma)_4](ClO_4)_4$(3$(ClO_4)_4$), $[Mn_4O_6(4,4'\text{-}Me_2bpma)_4]$-$(ClO_4)_4$ (4$(ClO_4)_4$), $[Mn_4O_6(5,5'\text{-}Me_2bpma)_4](ClO_4)_4$(5$(ClO_4)_4$). The preparation of **3**$(ClO_4)_4$ and related complexes **4**$(ClO_4)_4$ and **5**$(ClO_4)_4$ was entirely analogous to that used for the preparation of **1**$(ClO_4)_4$. See Supporting Information for experimental details. A compilation of synthesis yields, elemental analyses, and MS and IR spectral data for **3**$(ClO_4)_4$, **4**$(ClO_4)_4$, and **5**$(ClO_4)_4$ is given in Table S2.

(f) $[Mn_4O_6(bpea)_4](X)_3$ (2$(X)_3$, X = ClO_4^-, BF_4^-, $BAr'_4{}^-$). Synthesis of **2**, based on one-electron reduction of **1,** was performed under prepurified argon with standard Schlenk and drybox techniques. Compound **2** was prepared by two different methods.

Method A (2$(ClO_4)_3$). Bulk electrolysis of an acetonitrile solution (8.0 mL) of **1**$(ClO_4)_4$ (226 mg, 0.140 mmol) in 0.1 M TBAP at −0.1V produced the one-electron reduced complex **2**$(ClO_4)_3$. A typical reaction time for bulk electrolysis was 25 min (see Figure S1 for a plot of charge versus time). Partial separation of the electrolyte from **2** was achieved by precipitation of the bulk electrolysis solution (after concentrating to 3 mL) with 40 mL of tetrahydrofuran to produce a dark brown powder. This was redissolved in 2 mL of acetonitrile and reprecipitated by addition of 25 mL of tetrahydrofuran. An electrolyte-free sample of **2** was obtained after this last step was repeated three additional times. Drying in vacuo for 1 h produced 199 mg (94%). Anal. Calcd for $Mn_4Cl_3O_{18}C_{56}H_{68}N_{12}$: Mn, 14.43; C, 44.15; H, 4.50; N, 11.03; Cl, 6.98. Found: Mn, 14.42; C, 42.79; H, 4.35; N, 10.47; Cl, 6.62. Selected IR bands (cm^{-1}): 1605 (s), 1573 (m), 1480 (s), 1432 (s), 1391 (m), 1281 (m), 1156 (w), 1095 (vs), 1053 (sh), 1029 (s), 993 (w), 920 (w), 860 (w), 766 (s), 690 (m), 657 (w), 625 (s), 509 (w), 475 (w), 439 (w).

Method B (2$(BF_4)_3$) and 2$(BAr'_4)_3 \cdot 3C_2H_4Cl_2$. Compound **2** can also be prepared by reduction of **1**$(X)_4$ with Me_3tacn in acetonitrile (X = ClO_4^-, BF_4^-, $CF_3SO_3^-$, $BAr'_4{}^-$, and PF_6^-) or dichloroethane (X = $BAr'_4{}^-$). In a typical reaction 38 mg (0.22 mmol) of Me_3tacn was added to 232 mg (0.148 mmol) of **1**$(BF_4)_4$ in 8.0 mL of acetonitrile and the mixture was stirred. Transformation to **2**$(BF_4)_3$ is complete in about 5 min according to UV−vis spectrophotometry. Diffusion of diethyl ether at −36 °C produced a dark crystalline product which was collected by filtration (250 mg, 92% yield, assuming five CH_3CN molecules of crystallization). Drying of the finely ground product in vacuo for 1 h produced 184 mg (84%, assuming complete removal of solvent of crystallization). Anal. Calcd for $Mn_4O_6C_{56}H_{68}N_{12}B_3F_{12}$: Mn, 14.79; C, 45.28; H, 4.61; N, 11.31. Found: Mn, 14.61; C, 45.00; H, 4.67; N, 11.15.

Reduction of **1**$(BAr'_4)_4$ in dichloroethane leads to precipitation of **2**$(BAr'_4)_3$. In a typical reaction 32 mg (0.186 mmol) of Me_3tacn was added to 580 mg (0.124 mmol) of **1**$(BAr'_4)_4$ in 14 mL of dichloroethane and the mixture was stirred. Conversion to **2**$(BAr'_4)_3$ is complete upon mixing of the reactants, followed by slow precipitation from the reaction mixture. After the solution is concentrated to 3 mL under vacuum, **2**$(BAr'_4)_3$ is collected by filtration as a tan solid (336 mg, 66% yield, assuming three $C_2H_4Cl_2$ molecules of crystallization, after drying in vacuo for 30 min). Anal. Calcd for $Mn_4O_6C_{158}H_{116}N_{12}F_{72}Cl_6B_3$: Mn, 5.34; C, 46.16; H, 2.84; N, 4.09; F, 33.27. Found: Mn, 5.42; C, 45.82; H, 2.79; N, 4.18; F, 32.19.

NMR Titration. Protonation of 1$(CF_3SO_3)_4$, 3$(ClO_4)_4$, 4$(ClO_4)_4$, and 5$(ClO_4)_4$. In a typical titration, a solution of **1**$(CF_3SO_3)_4$ in CD_3CN (21 mM, based on 15 mg, 8.2 μmol, in 0.4 mL) was prepared and transferred to an NMR tube in the glovebox. Protonation of **1**$(CF_3SO_3)_4$ was accomplished outside the box by addition of aliquots of CF_3SO_3H (0.5 μL, 5.7 μmol) with a gastight syringe through the septum seal of the NMR tube. Generation of **1**H$(CF_3SO_3)_5$ was considered complete when additional aliquots of CF_3SO_3H produced no further change in the ^1H NMR spectrum. For comparison, titration of **1**$(ClO_4)_4$ in this manner exhibited a similar "endpoint" and ^1H NMR spectral features. Titration of the perchlorate salts of **3**−**5** was entirely analogous to that of **1**$(CF_3SO_3)_4$.

Spectrophotometric Titration. Protonation of 1$(CF_3SO_3)_4$. In a typical titration, a 1.2 mL aliquot of a stock solution of **1**$(CF_3SO_3)_4$ in CH_3CN (5.74×10^{-4} M, based on 26.1 mg (14.4 μmol) in a 25 mL volumetric flask) was prepared and transferred to a gastight cuvette in the glovebox. Protonation of **1**$(CF_3SO_3)_4$ was accomplished outside the box by addition of aliquots of CF_3SO_3H (1.0 μL, 11 μmol) with a gastight syringe through the septum seal of the cuvette. Generation of **1**H$(CF_3SO_3)_5$ was considered complete when additional aliquots of CF_3SO_3H produced no further change in the UV−vis spectrum.

X-ray Crystallography. (a) $[Mn_4O_6(bpea)_4](ClO_4)_4$(1$(ClO_4)_4$). The compound crystallizes as $[Mn_4O_6(bpea)_4](ClO_4)_4 \cdot 5CH_3CN$ in the triclinic space group $P\bar{1}$ with two molecules in the unit cell. Relevant crystal data are summarized in Table 1. Single crystals suitable for structure determination were obtained by diffusion of diethyl ether into an acetonitrile solution of **1**$(ClO_4)_4$ at −36 °C. A black, prismatic crystal of suitable dimensions was taken from the mother liquor, coated with Paratone-N oil, mounted on a glass fiber, and immediately

transferred to the dinitrogen cold stream. Data were collected at 183 K with Mo Kα radiation ($\lambda = 0.71073$ Å) on a Siemens SMART CCD area-detector diffractometer out to $2\theta_{max} = 56.58°$, yielding a total of 24 783 measured reflections of which 17 410 were unique ($R_{int} = 0.0357$, semiempirical absorption corrections). The structure was solved by direct methods and refined by full-matrix least-squares methods on F^2 with statistical weighting, anisotropic displacement parameters for all non-hydrogen atoms (including disordered methylene carbons (C6 and C9) on one bpea moiety), and constrained isotropic H atoms to give $R_1 = \{\Sigma[w(F_o^2 - F_c^2)^2]/\Sigma[w(F_o^2)^2]\}^{1/2} = 0.0936$ on all data, conventional $R_1 = 0.0821$ on $F_o^2 > 2\sigma F_o^2$, goodness of fit $S = 1.094$ for all F^2 values and 1046 refined parameters. Final difference map features, within 1.686 and −1.896 e Å^{-3}, were primarily associated with lattice solvate. Programs employed were Siemens SMART[58] and SAINT[59] control and integration software, and Siemens SHELXTL-PLUS[60] structure solution and refinement software.

(b) $[Mn_4O_6(bpea)_4](BF_4)_3(2(BF_4)_3)$. The compound crystallizes as $[Mn_4O_6(bpea)_4](BF_4)_3 \cdot 5CH_3CN$ in the triclinic space group $P\bar{1}$ with two molecules in the unit cell. Relevant crystal data are summarized in Table 1. Single crystals were grown by diffusion of diethyl ether into an acetonitrile solution of **2**$(BF_4)_3$ (see preparation method B above) at −36 °C under argon. A black crystal of suitable dimensions was taken from the mother liquor, coated with Paratone-N oil, mounted on a glass fiber, and immediately transferred to the dinitrogen cold stream. A total of 10 646 reflections were measured, of which 10 613 were unique ($R_{int} = 0.0490$, semiempirical absorption corrections). The structure was solved as above to give $R_1 = \{\Sigma[w(F_o^2 - F_c^2)^2]/\Sigma[w(F_o^2)^2]\}^{1/2} = 0.1242$ on all data, conventional $R_1 = 0.1013$ on $F_o^2 > 2\sigma F_o^2$, goodness of fit $S = 1.190$ for all F^2 values and 973 refined parameters. Final difference map features were within 0.763 and −0.731 e Å^{-3}.

Results and Discussion

Synthesis. Previous syntheses of discrete high valent manganese-oxo complexes, including the $[Mn_4O_6(tacn)_4]^{4+}$ (**6**)[20,21] and $[Mn_4O_5(OH)(tame)_4]^{5+}$ (**7**)[22] aggregates, utilized air oxidation of basic solutions of Mn^{II} and free ligand to "assemble" the thermodynamically stable adamantane-like core. Although attempts to adopt this methodology for the bpea ligand system failed, a comproportionation reaction of Mn^{II} and Mn^{VII} starting materials was successful in obtaining a tetranuclear product in the Mn^{IV} state. Although all reaction conditions have not been exhaustively varied, the procedure has been optimized to give consistent yields of **1**$(ClO_4)_4$.[61]

In the course of exploring terminal ligand substitution chemistry of **1** we observed that a solution of **1**$(ClO_4)_4$ in acetonitrile reacts with Me_3tacn at room temperature to generate **2**$(ClO_4)_3$.[62] Subsequently, we showed that other tertiary amines, as well as $Fe(Cp^*)_2$, are effective one-electron reductants of

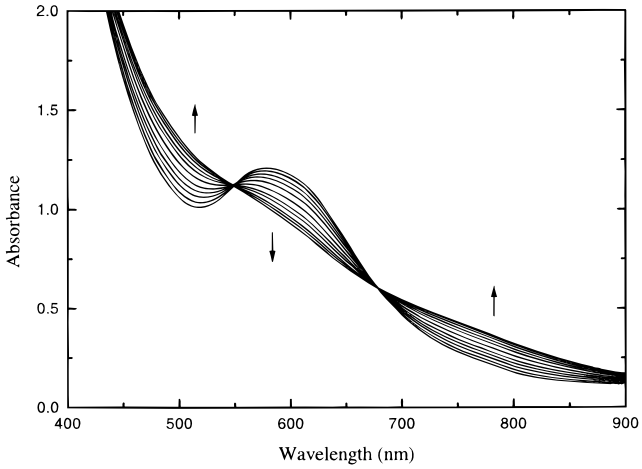

Figure 2. Spectrophotometric titration of $[Mn_4O_6(bpea)_4](ClO_4)_4$ (**1**$(ClO_4)_4$) (initial spectrum) with Me_3tacn to generate $[Mn_4O_6(bpea)_4](ClO_4)_3$ (**2**$(ClO_4)_4$). Isosbestic points at 550 and 680 nm. Spectra were recorded after sequential additions of Me_3tacn (0.12 equivalents) to **1**$(ClO_4)_4$ (0.603 mM) in CH_3CN under argon.

1.[63] Titration of **1** in acetonitrile with Me_3tacn or $Fe(Cp^*)_2$ can be followed by ^{1}H NMR (Figure S2) and UV−vis spectrophotometry (Figure 2).[64] The reaction of **1**$(ClO_4)_4$ with $Fe(Cp^*)_2$ in acetonitrile is described by reaction 1.

$$[Mn_4O_6(bpea)_4]^{4+} + [Fe(Cp^*)_2] \rightleftharpoons [Mn_4O_6(bpea)_4]^{3+} + [Fe(Cp^*)_2]^{+} \quad (1)$$

Near-quantitative conversion of **1** to **2** (94% isolated yield) by bulk coulometry, with $n = 0.95$, (Figure S1, plot of charge versus time) corroborates the assignment of **2** as the one-electron reduced species. Stability of complex **2** sufficient for isolation and characterization can be attributed to the donor properties of the bpea ligand. Unlike the strongly basic donor ligands tacn and tame, which stabilize the higher oxidation state of the Mn cluster (vide infra), the weaker donor nature of bpea facilitates isolation of the $\{Mn_4O_6\}$ core in the $(IV)_4$ *and* $(III)(IV)_3$ oxidation states.

Structures. The Mn and O atoms in the crystal structure of **1** (Figure 3a) define the adamantane skeleton.[65] The Mn atoms occupy the apexes of a tetrahedron and the O atoms occupy the apexes of an octahedron. Each Mn atom is coordinated to three bridging O atoms and three N atoms from the bpea ligand in a psuedooctahedral geometry. Unlike the near-T_d point symmetry observed for $[Mn_4O_6(tacn)_4]^{4+}$, the cation $[Mn_4O_6(bpea)_4]^{4+}$ approaches only S_4 point symmetry because of the relatively low symmetry of the facially coordinated bpea ligand. Although the tacn ligand displays local 3-fold symmetric coordination to the manganese ions in **6**, with an average Mn−N

(58) SMART, v 4.A50, Siemens Molecular Analytical Research Tool; Siemens Analytical X-ray Instruments, Inc., Madison, WI, 1995.

(59) SAINT, Data Reduction Software for Single-Crystal Diffraction with an Area Detector; Siemens Analytical X-ray Instruments, Inc., Madison, WI, 1995.

(60) SHELXTL-PLUS v 5.0; Siemens Industrial Automation Inc., Analytical Instrumentation, Madison, WI, 1995.

(61) The optimal ratio of Mn(II):Mn(VII) starting reagents was found to be 3:2 yielding an average oxidation state of +4.0. Experiments designed to optimize the yield of **1**$(ClO_4)_4$ as a function of reaction time indicated that aggregation was essentially complete within 1 h; times longer than 6 h produced a significant decrease in the yield of **1**$(ClO_4)_4$.

(62) ^{1}H NMR showed that the corresponding oxidation of Me_3tacn in acetonitrile-d_3 under argon generated $[Me_3tacnH][ClO_4]$ by way of comparison with a spectrum of an authentic sample of $[Me_3tacnH][CF_3SO_3]$. Under similar conditions (argon ambient and rigorously dried solvent) oxidation of Me_3tacn with $[NO][BF_4]$ generated $[Me_3tacnH][BF_4]$. The source of the H-atom is unknown at this time.

(63) Although among amines Me_3tacn is the most efficient one-electron reductant, requiring 1.2 equivalents of Me_3tacn for quantitative conversion of **1** to **2**, other tertiary amines, including triethylamine, *N*,*N*,*N*′,*N*′,*N*′-pentamethyldiethylenetriamine, quinuclidine, proton sponge, and DABCO, were effective reductants at somewhat higher concentrations. Triethylamine has been used previously in the reduction of inorganic complexes (Connelly, N. G.; Geiger, W. E. *Chem. Rev.* **1996**, *96*, 877−910). The redox chemistry of tertiary amines has been extensively reviewed (Weinberg, N. L.; Weinberg H. R. *Chem. Rev.* **1968**, *68*, 449−522).

(64) The final spectrum corresponds to that of **2**$(BF_4)_3$ plus $[Me_3tacnH][BF_4]$ in acetonitrile. Measurable absorbance due to Me_3tacnH^+ is found for wavelengths less than 400 nm. The spectrum shown in Figure 2 is in good agreement with that of an authentic spectrum of **2** prepared by bulk electrolysis.

(65) In principle, the tetranuclear cation $[Mn_4O_6(bpea)_4]^{4+}$ can exist in many possible isomeric forms, yet remarkably, only one is observed in the solid state or in solution.

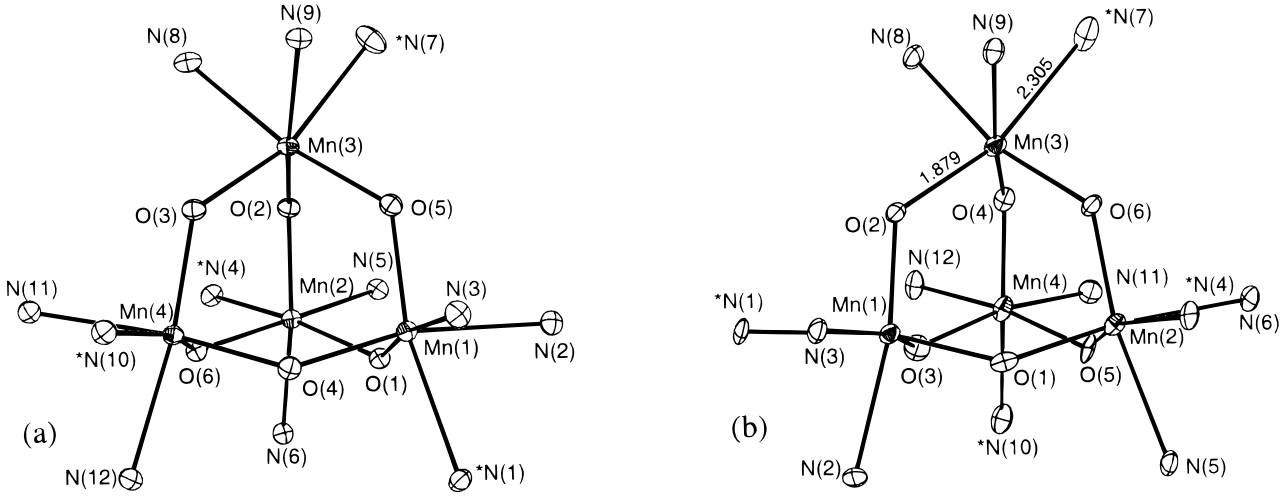

Figure 3. ORTEP plots of the structures and atom labeling schemes of the cation cores of (a) $[Mn_4O_6(bpea)_4](ClO_4)_4 \cdot 5CH_3CN$ (**1**$(ClO_4)_4 \cdot 5CH_3CN$) and (b) $[Mn_4O_6(bpea)_4](BF_4)_3 \cdot 5CH_3CN$ (**2**$(BF_4)_3 \cdot 5CH_3CN$), showing 30% probability thermal ellipsoids. *N designates alkyl nitrogen atoms. The Mn^{III} ion in **2**$(BF_4)_3 \cdot 5CH_3CN$ is Mn(3) and the bond lengths of the Jahn−Teller axis (O(2)−Mn(3)−N(7)) are labeled. For clarity, carbon and hydrogen atoms are omitted. More complete ORTEP plots of **1**$(ClO_4)_4 \cdot 5CH_3CN$ and **2**$(BF_4)_3 \cdot 5CH_3CN$ are given in Figures S3 and S4, respectively.

Table 2. Selected Bond Distances (Å) and Angles (°) for $[Mn_4O_6(bpea)_4](ClO_4)_4 \cdot 5CH_3CN$ (**1**$(ClO_4)_4 \cdot 5CH_3CN$)

bond distances			
Mn(1)−Mn(3)	3.243(2)	Mn(2)−Mn(4)	3.245(2)
Mn(1)−Mn(4)	3.254(2)	Mn(2)−Mn(1)	3.239(2)
Mn(2)−Mn(3)	3.243(2)	Mn(3)−Mn(4)	3.255(2)
Mn(4)−O(4)	1.781(3)	Mn(2)−O(2)	1.783(3)
Mn(4)−O(3)	1.791(3)	Mn(2)−O(1)	1.802(3)
Mn(4)−O(6)	1.798(3)	Mn(2)−O(6)	1.815(3)
Mn(4)−N(12)	2.085(4)	Mn(2)−N(5)	2.090(4)
Mn(4)−N(11)	2.106(4)	Mn(2)−N(6)	2.106(4)
Mn(4)−N(10)	2.169(4)	Mn(2)−N(4)	2.196(4)
Mn(3)−O(2)	1.787(3)	Mn(1)−O(4)	1.794(3)
Mn(3)−O(5)	1.808(3)	Mn(1)−O(1)	1.805(3)
Mn(3)−O(3)	1.821(3)	Mn(1)−O(5)	1.810(3)
Mn(3)−N(8)	2.092(4)	Mn(1)−N(3)	2.093(4)
Mn(3)−N(9)	2.110(4)	Mn(1)−N(2)	2.107(4)
Mn(3)−N(7)	2.212(4)	Mn(1)−N(1)	2.207(4)
bond angles			
O(4)−Mn(4)−O(3)	94.9(1)	O(4)−Mn(1)−O(1)	95.0(1)
O(4)−Mn(4)−O(6)	99.6(1)	O(4)−Mn(1)−O(5)	101.3(1)
O(3)−Mn(4)−O(6)	99.2(1)	O(1)−Mn(1)−O(5)	98.02(1)
O(2)−Mn(3)−O(5)	94.9(1)	Mn(4)−O(6)−Mn(2)	127.9(2)
O(2)−Mn(3)−O(3)	99.6(1)	Mn(2)−O(1)−Mn(1)	127.7(2)
O(5)−Mn(3)−O(3)	99.1(1)	Mn(4)−O(3)−Mn(3)	128.6(2)
O(2)−Mn(2)−O(1)	100.8(1)	Mn(3)−O(5)−Mn(1)	127.4(2)
O(2)−Mn(2)−O(6)	95.6(1)	Mn(4)−O(4)−Mn(1)	131.0(2)
O(1)−Mn(2)−O(6)	98.4(1)	Mn(2)−O(2)−Mn(3)	130.5(2)

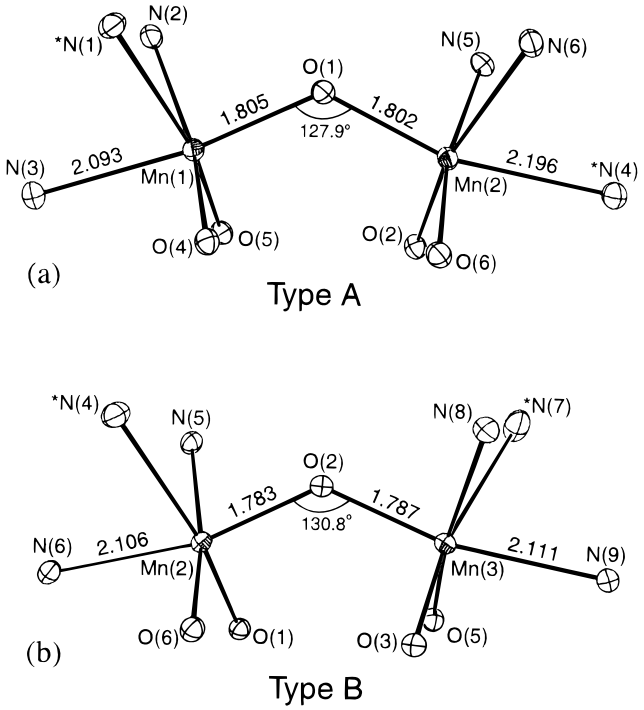

Figure 4. ORTEP plots (30% probability thermal ellipsoids) of representative portions of the $[Mn_4O_6(bpea)_4](ClO_4)_4 \cdot 5CH_3CN$ (**1**$(ClO_4)_4 \cdot 5CH_3CN$) cation illustrating (a) a longer Mn−N_{alkyl} bond and a type A Mn−N_{py} bond and Mn−O−Mn bridge, and (b) type B Mn−N_{py} bonds and Mn−O−Mn bridge. *N designates alkyl nitrogen atoms. For clarity, carbon and hydrogen atoms are omitted. The bond lengths of the selected bonds and angles (see Table 2 for a more complete data set) closely match the average bond lengths and angles for each type of bond in **1**$(ClO_4)_4 \cdot 5CH_3CN$.

distance of 2.086 Å,[21] the combination of tertiary amine and pyridyl nitrogen moieties results in three distinct types of Mn−N bond distances (Table 2): an average Mn−N_{alkyl} bond length of 2.196(2) Å and two kinds of Mn−N_{py} bonds; a "short" Mn−N_{py} bond (type A, Figure 4a) with an average length of 2.090(2) Å and a longer Mn−N_{py} bond (type B, Figure 4b) with an average length of 2.108(2) Å. Longer Mn−N_{alkyl} bonds[66] are observed for other structurally characterized compounds with the bpea[42,44,45] and bpta[42] ligands, as well as with the bispicen[67,68] and tmpa[69] ligands. In general, for ancillary ligands with different donor type atoms, the stronger donor atoms would be expected to have the shorter metal−ligand bond lengths, resulting in Mn−N_{alkyl} bonds slightly shorter than the Mn−N_{py} bonds. Such is the case for dinuclear hydroxo-bridged Cr^{III} complexes containing bispicen[70] and bispictn[71] ligands. The

(66) The comparison is among Mn^{IV}-N_{alkyl} and Mn^{IV}-N_{py} which are trans to μ-O ligands.

(67) Collins, M. A.; Hodgson, D. J.; Michelson, K.; Towle, D. K. *J. Chem. Soc., Chem. Commun.* **1987**, 1659−1660.

(68) Goodson, P. A.; Glerup, J.; Hodgson, D. J.; Michelsen, K.; Pedersen, E. *Inorg. Chem.* **1990**, *29*, 503−508.

(69) Towle, D. K.; Botsford, C. A.; Hodgson, D. *Inorg. Chim. Acta* **1988**, *141*, 167−168.

(70) Heinrichs, M. A.; Hodgson, D. J.; Michelsen, K.; Pedersen, E. *Inorg. Chem.* **1984**, *23*, 3174−3180.

(71) Fischer, H. R.; Hodgson, D. J.; Michelsen, K.; Pedersen, E. *Inorg. Chim. Acta* **1984**, *88*, 143−150.

crystallographic data of structurally characterized Mn complexes are, however, contrary to this expectation. It is probable that a competing interaction of steric and electronic factors for this ligand type is responsible for the observed structural trend among Mn complexes.

The S_4 symmetry of the $[Mn_4O_6(bpea)_4]^{4+}$ cation also results in inequivalent oxo ligands. The four oxo-bridges lying in the plane perpendicular to the pseudo C_2 axis of the $[Mn_4O_6(bpea)_4]^{4+}$ core (type A, Figure 4a) are characterized by an average Mn−O_{oxo} bond length of 1.806(1) Å and an average Mn−O−Mn angle of 127.9(1)°. The remaining two oxo-bridges lying on the C_2 axis (type B, Figure 4b) consist of slightly shorter Mn−O_{oxo} bonds (1.786(2) Å) and slightly larger Mn−O−Mn angles (130.8(1)°). These Mn−O_{oxo} distances and Mn−O−Mn angles are very similar to those found in **6** (1.797 Å and 128.0°, respectively) and are generally consistent with metric data for other Mn^{IV}-O_{oxo} complexes.

The average Mn···Mn distance of **1** (3.248 Å) is slightly longer than the corresponding distance in **6** (3.226 Å) and is similar in length to the distance between the apical and basal manganese ions in the $\{Mn^{IV}_3O_4\}$ aggregates (3.184−3.256 Å).[45,72,73] The Mn···Mn distance of **1** is consistent with the trend that as the number of bridging oxides between Mn ion pairs decreases, the metal−metal distance increases.[74] Thus, although the Mn···Mn distance for the $\{Mn^{IV}_2(\mu\text{-}O)_3\}$ aggregate is 2.296 Å,[21] the range within $\{Mn^{IV}_2(\mu\text{-}O)_2\}$ units is understandably longer (2.580−2.757 Å),[75] and the $\{Mn^{IV}_3O_4\}$ and $\{Mn^{IV}_4O_6\}$ vectors are longer still.

The crystal structure of the one-electron reduced mixed-valence analog of $[Mn_4O_6(bpea)_4]^{4+}$, complex **2**, also contains the adamantane skeleton (Figure 3b). Unlike the approximate S_4 symmetry of the $(Mn^{IV})_4$ cluster, in which the Mn atoms are symmetry related, the $(Mn^{III})(Mn^{IV})_3$ cluster contains a crystallographically distinct Mn^{III} ion (Mn(3) in Table 3). The Mn^{III} ion is distinguishable from the Mn^{IV} ions based on a comparison of bond distances (Table 3). Distortion along the N(7)−Mn-(3)−O(2) axis is illustrated by an elongated Mn−N_{alkyl} bond (2.305 Å) and an elongated type A Mn−O bond (1.878 Å), and is consistent with an axial distortion predicted by the Jahn−Teller theorem for a high-spin d^4 ion. Because compound **2** exhibits the same overall stereochemistry as that found in **1**, and because there is no 3-fold rotation axis through the Mn^{III} ion relating the Mn^{IV} ions, **2** has no imposed symmetry in the solid state. The previously noted trends of longer Mn−N_{alkyl} bonds and the two types of Mn−N_{py} bonds are observed for the Mn^{IV} ions of **2** as well. The two different types of oxo ligands found in **1** are also observed for the Mn^{IV} ions of **2**, however, all three of the oxo ligands bound to the Mn^{III} center are inequivalent. Thus, although two types of oxo ligands bridge the Mn^{IV} centers in **1**, there are five types of bridging oxo ligands in **2**.

Physical Properties. Electrospray mass spectrometry of **1**$(ClO_4)_4$ (Figure S5) clearly reveals the $[Mn_4O_6(bpea)_4](ClO_4)_3^+$ ion at *m*/*z* 1524, as well as the intense fragments at *m*/*z* 969, 696, and 227, corresponding to $[Mn_4O_6(bpea)_2](ClO_4)_2^+$, $[Mn_2O_2(bpea)_2](ClO_4)^+$, and $bpea^+$, respectively. Comparison of the electrospray mass spectrometry of **2**$(ClO_4)_3$ (Figure S6) with that of **1**$(ClO_4)_4$ reveals that **2**$(ClO_4)_3$ features a prominent fragment at *m*/*z* 1424, corresponding to the $Mn^{III}(Mn^{IV})_3$ species $[Mn_4O_6(bpea)_4](ClO_4)_2^+$, and the *m*/*z* 1524 peak characteristic of the $(Mn^{IV})_4$ species is noticeably absent. The spectra of **1**$(ClO_4)_4$ and **2**$(ClO_4)_3$ are otherwise similar. These data indicate that the $[Mn_4O_6(bpea)_4](ClO_4)_4$ aggregate can undergo significant gas phase fragmentation under relatively mild ionization conditions. In contrast, the electrospray mass spectrum of $[Mn_4O_6(tacn)_4](ClO_4)_4$(**6**$(ClO_4)_4$) (Figure S7) demonstrates a relatively inert core, because the predominant peaks correspond to the intact core with sequential loss of counterions ($[Mn_4O_6(tacn)_4](ClO_4)_3^+$, *m*/*z* 1131; $[Mn_4O_6(tacn)_4](ClO_4)_2^{2+}$, *m*/*z* 515).

Table 3. Selected Bond Distances (Å) and Angles (°) for $[Mn_4O_6(bpea)_4](BF_4)_3{\cdot}5CH_3CN$ (**2**$(BF_4)_3{\cdot}5CH_3CN$)

bond distances			
Mn(1)−Mn(3)	3.253(2)	Mn(2)−Mn(4)	3.229(2)
Mn(1)−Mn(4)	3.252(2)	Mn(2)−Mn(1)	3.237(2)
Mn(2)−Mn(3)	3.244(2)	Mn(3)−Mn(4)	3.236(2)
Mn(1)−O(2)	1.773(5)	Mn(3)−O(4)	1.807(6)
Mn(1)−O(3)	1.788(6)	Mn(3)−O(6)	1.809(6)
Mn(1)−O(1)	1.815(6)	Mn(3)−O(2)	1.878(6)
Mn(1)−N(2)	2.120(6)	Mn(3)−N(9)	2.127(8)
Mn(1)−N(3)	2.122(8)	Mn(3)−N(8)	2.128(9)
Mn(1)−N(1)	2.221(8)	Mn(3)−N(7)	2.30(1)
Mn(2)−O(6)	1.767(5)	Mn(4)−O(3)	1.791(7)
Mn(2)−O(1)	1.799(7)	Mn(4)−O(5)	1.797(6)
Mn(2)−O(5)	1.806(5)	Mn(4)−O(4)	1.810(6)
Mn(2)−N(6)	2.094(9)	Mn(4)−N(12)	2.113(8)
Mn(2)−N(5)	2.135(7)	Mn(4)−N(11)	2.150(9)
Mn(2)−N(4)	2.204(4)	Mn(4)−N(10)	2.231(9)
bond angles			
O(2)−Mn(1)−O(3)	96.6(3)	O(3)−Mn(4)−O(5)	94.4(3)
O(2)−Mn(1)−O(1)	100.1(3)	O(3)−Mn(4)−O(4)	100.8(3)
O(3)−Mn(4)−O(1)	100.0(3)	O(5)−Mn(4)−O(4)	100.4(3)
O(6)−Mn(2)−O(1)	96.4(3)	Mn(2)−O(6)−Mn(3)	130.3(3)
O(6)−Mn(2)−O(5)	101.4(3)	Mn(1)−O(2)−Mn(3)	126.0(4)
O(1)−Mn(2)−O(5)	98.5(3)	Mn(4)−O(5)−Mn(2)	127.3(4)
O(4)−Mn(3)−O(6)	95.6(3)	Mn(1)−O(3)−Mn(4)	130.6(3)
O(4)−Mn(3)−O(2)	99.5(3)	Mn(3)−O(4)−Mn(4)	126.9(3)
O(6)−Mn(3)−O(2)	99.9(3)	Mn(2)−O(1)−Mn(1)	127.2(3)

The IR spectrum of **1** shows a number of bands attributable to the bpea ligands and an intense band at 709 cm^{-1}. ^{18}O enrichment (see Experimental Section) results in an observable shift of only the 709 cm^{-1} band to 675 cm^{-1}, providing a definitive assignment of this band as a Mn−O−Mn stretch. Previous analysis of the vibrational spectrum of the structurally related core of **6** resulted in the assignment of a band at 730 cm^{-1} to a Mn−O−Mn stretch. A number of higher valent metal adamantane-like aggregates also display bands in this region[76−80] (see Table S3 for a compilation of selected structural and vibrational data). Comparison of the IR spectra of **1**$(ClO_4)_4$ and **2**$(ClO_4)_3$ reveals that the major difference is a decrease in energy of the Mn−O−Mn stretch from 709 to 692 cm^{-1}, concomitant with a reduction in its intensity, following one-electron reduction of the $\{Mn_4O_6\}^{4+}$ core.

The electronic spectrum of **1** in acetonitrile displays bands characteristic of the adamantane-like $\{Mn_4O_6\}^{4+}$ core.[81] Maxima are observed at 1014 nm (ϵ = 270 $M^{-1}cm^{-1}$), 580 nm (ϵ =

(72) Auger, N.; Girerd, J.-J.; Corbella, M.; Gleizes, A.; Zimmermann, J. L. *J. Am. Chem. Soc.* **1990**, *112*, 448−450.
(73) Sarneski, J. E.; Thorp, H. H.; Brudvig, G. W.; Crabtree, R. H.; Schulye, G. K. *J. Am. Chem. Soc.* **1990**, *112*, 7255−7260.
(74) Larson, E.; Lah, M. S.; Li, X.; Bonadies, J. A.; Pecoraro, V. L. *Inorg. Chem.* **1992**, *31*, 373−378.
(75) Manchanda, R.; Brudvig, G. W.; Crabtree, R. H. *Coord. Chem. Rev.* **1995**, *144*, 1−38.
(76) Murch, B. P.; Bradley, F. C.; Boyle, P. D.; Papaefthymiou, V.; Que, L. *J. Am. Chem. Soc.* **1987**, *109*, 7993−8003.
(77) Wieghardt, K.; Ventur, D.; Tsai, Y. H.; Kruger, C. *Inorg. Chim. Acta* **1985**, *99*, L25-L27.
(78) Sala-Pala, J.; Guerchais, J.-E.; Edwards, A. J. *Angew. Chem., Int. Ed. Engl.* **1982**, *21*, 870−871.
(79) Drueke, S.; Wieghardt, K.; Nuber, B.; Weiss, J.; Bominaar, E. L.; Sawaryn, A.; Winkler, H.; Trautwein, A. X. *J. Am. Chem. Soc.* **1989**, *111*, 4477−4483.
(80) Sessler, J. L.; Sibert, J. W.; Burrell, A. K.; Lynch, V.; Markert, J. T.; Wooten, C. L. *Inorg. Chem.* **1993**, *32*, 4277−4283.

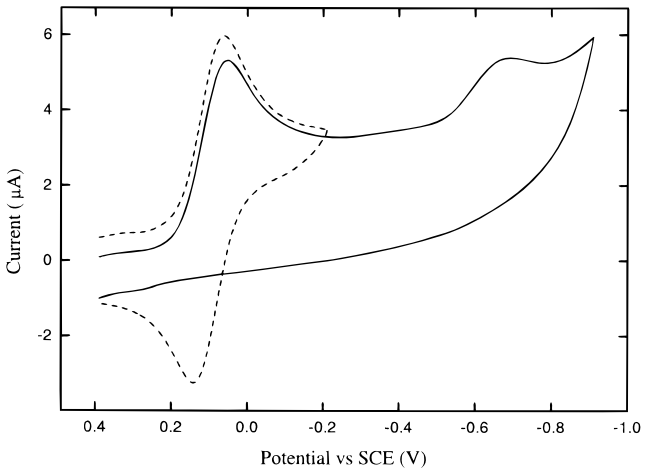

Figure 5. Cyclic voltammograms of $[Mn_4O_6(bpea)_4](ClO_4)_4$ (**1**$(ClO_4)_4$) (1.20 mM) in 0.2 M TBAP in acetonitrile (scan rate of 50 mV/s) illustrating the quasi-reversible redox couple (---) and the irreversible reduction (—).

2070 $M^{-1}cm^{-1}$), and 355 nm (sh). Based on the spectral analysis of a number of $\{Mn^{III}Mn^{IV}(\mu\text{-}O)_2\}^{3+}$ complexes,[82] and a shift of similar bands to higher energy for related $\{(Mn^{IV})_2(\mu\text{-}O)_2\}^{4+}$ complexes,[82] the absorption at 580 nm is tentatively assigned to an oxo-to-manganese(IV) charge transfer band (LMCT). This assignment is supported by comparison of the previously reported electronic structure of the adamantane-like complexes **6** and **7,** for which the putative LMCT band is shifted to 552 and 548 nm, respectively. The shift to higher energy of this LMCT band for the tacn and tame complexes relative to the bpea complex is consistent with an increase of the relevant d-orbital energy in **6** and **7** in relation to **1**, arising from the more basic tacn and tame ligands.

A deep green acetonitrile solution of **1** changes to black-brown, characteristic of **2,** following one-electron reduction by Me_3tacn. The prominent LMCT band for **1** at 580 nm disappears in the conversion to **2**, rendering the electronic spectrum of **2** somewhat nondescript (Figure 2).

Cyclic Voltammetry. Cyclic voltammetric studies of **1**$(ClO_4)_4$ in acetonitrile at a scan rate of 50 mV s^{-1}, shown in Figure 5, display one quasi-reversible redox couple at $E_{1/2} = 0.104$ V ($\Delta E_p = 68$ mV) and an irreversible reduction at $E_p = -0.628$ V versus SCE corresponding to the IV,IV,IV,IV/III,IV,IV,IV and III,IV,IV,IV/III,III,IV,IV couples, respectively.[83] The electrochemical behavior of **1** can be contrasted to that previously reported for the adamantane-shaped cores **6** and **7**.[40] The more basic ligands such as tacn and tame are stronger N-atom donor ligands than the bpea ligand, and are expected to better stabilize the higher oxidation state of the Mn cluster. This is supported by a positive shift in potential of 780 mV for the IV,IV, IV, IV/III,IV,IV,IV couple from **6** to **1** and 700 mV from **7** to **1**. Given the large positive shift in potential for the one-electron reduction couple in **1**, it is not surprising that there is not an observed oxidative wave, because it would likely be shifted out of the electrochemical window of acetonitrile (±2.5 V).[84] A quasi-reversible wave at $E_{1/2} = 0.102$ V ($\Delta E_p = 78$ mV) is observed if an acetonitrile solution of **2**$(ClO_4)_3$ is scanned in the negative direction from +0.25 V, consistent with the formulation of **2** as the product of a one-electron reduction of **1**.

Magnetic Susceptibility. Magnetic susceptibility measurements on a powdered sample of **1** were conducted in the temperature range 6−300 K at a constant applied magnetic field of 0.5 T. The effective magnetic moment (μ_{eff}/Mn) of **1** is 5.69 μ_B at 6 K, which increases up to 5.78 μ_B at 15 K and then gradually decreases to 4.44 μ_B at 300 K (Figure S8). A solution magnetic susceptibility value of μ_{eff}/Mn for **1**$(CF_3SO_3)_4$ of 4.67 μ_B at 295 K is in reasonably good agreement with the solid-state value. The solution and solid-state values suggest that **1** experiences overall ferromagnetic coupling,[85] similar to that previously reported for **6**.[20,22] The net ferromagnetic coupling of the Mn^{IV} ions in the adamantane-shaped clusters has been attributed to either intrinsic pairwise ferromagnetism [22] or "spin frustration"[86] arising from the T_d symmetry of the $\{Mn_4O_6\}^{4+}$ cation.[87] The magnetic behavior of **1** and **6** is unusual among the known tetranuclear manganese-oxo aggregates,[75,87,88] and is the subject of an ongoing investigation.[89] Interestingly, the solution magnetic susceptibility of an acetonitrile solution of **2**$(ClO_4)_3$ prepared by bulk coulometry (μ_{eff}/Mn of 3.19 μ_B at 295 K) indicates that the conversion of **1** to **2** is attendant with a change from net ferromagnetic coupling to overall moderate antiferromagentic coupling within the manganese-oxo core. It is noteworthy that the change in magnetic moment accompanying oxidation of **2** to **1** bears some similarity to the change in magnetic moment observed for S-state advancement of PSII core complexes. Oxidation of the OEC from S_1 to S_2, thought to involve a one-electron oxidation of the manganese aggregate,[3,19] is marked by an increase in the effective magnetic moment, given by $\Delta\mu^2$, of 9−17 $\mu_B{}^2$.[38,39] A one-electron oxidation of **2** to **1** has a $\Delta\mu^2$ value of 38.2 $\mu_B{}^2$, which has the same sign as that observed for the $S_1 \rightarrow S_2$ transition in PSII, but is somewhat greater in magnitude. Furthermore, oxidation of **2** to **1** involves only a modest structural change of the $\{Mn_4O_6\}$ cation. Likewise, one-electron oxidation of the OEC for the $S_1 \rightarrow S_2$ transition is believed to involve very little structural rearrangement.[7,90]

^{1}H NMR. The ^{1}H NMR spectra of **1**$(ClO_4)_4$ and **2**$(BF_4)_3$, shown in Figures 6a and 6b, respectively, can be understood in terms of their magnetic properties and the cation symmetry displayed in the solid state, in which the bpea ligands are equivalent only if effective S_4 symmetry is assumed. The bpea ligand of **1** and **2** consists of 14 inequivalent protons, of which 8 arise from inequivalent ring protons. The observed spectral inequivalence of the pyridyl rings of the bpea ligand most likely arises from two different Mn−N_{py} bond lengths (type A and B, Figure 4). A possible consequence of a shorter Mn−N_{py} bond is that the pyridyl ring is more tightly coupled to the core and

(81) λ_{max} values of the most prominent band for other $\{Mn_4O_6\}^{4+}$ cores include: $[Mn_4O_6(tame)_4]^{4+}$, $\lambda_{max} = 548$ nm (Hagen, K. S.; Westmoreland, T. D.; Scott, M. J.; Armstrong, W. H. *J. Am. Chem. Soc.* **1989**, *111*, 1907−1909) $[Mn_4O_6(tacn)_4]^{4+}$, $\lambda_{max} = 552$ nm (Wieghardt, K.; Bossek, U.; Gebert, W. *Angew. Chem., Int. Ed. Engl.* **1983**, *22*, 328−329).

(82) Gamelin, D. R.; Krik, M. L.; Stemmler, T. L.; Pal, S.; Armstrong, W. H.; Penner-Hahn, J. E.; Solomon, E. I. *J. Am. Chem. Soc.* **1994**, *116*, 2392−2399.

(83) A reversible electron transfer is characterized by a separation of cathodic and anodic CV peak potentials of 59/*n* mV, quasi-reversibility is characterized by cathodic and anodic peak potentials separated by more than 59/*n* mV, and irreversibility by the disappearance of a reverse peak (*n* = the number of electrons). A reversible electron transfer is also distinguished by a peak cathodic current/peak anodic current ratio of 1.

(84) Bard, A. J.; Faulkner, L. R. *Electrochemical Methods*; John Wiley and Sons: New York, 1980.

(85) For comparison, the spin-only magnetic moment of an uncoupled high spin d^3 ion is 3.87 μ_B.

(86) Kahn, O. *Molecular Magnetism*; VCH: New York, 1993.

(87) Thorp, H. H.; Brudvig, G. W. *New J. Chem.* **1991**, *15*, 479−490.

(88) Wieghardt, K. *Angew. Chem., Int. Ed. Engl.* **1989**, *28*, 1153−1172.

(89) We are currently pursuing a collaboration with Professor Dante Gatteschi (University of Florence) to develop an understanding of the ferromagnetic coupling in the $\{Mn_4O_6\}^{4+}$ cores.

(90) Liang, W.; Latimer, M. J.; Dau, H.; Roelofs, T. A.; Yachandra, V. K.; Sauer, K.; Klein, M. P. *Biochemistry* **1994**, *33*, 4923−4932.

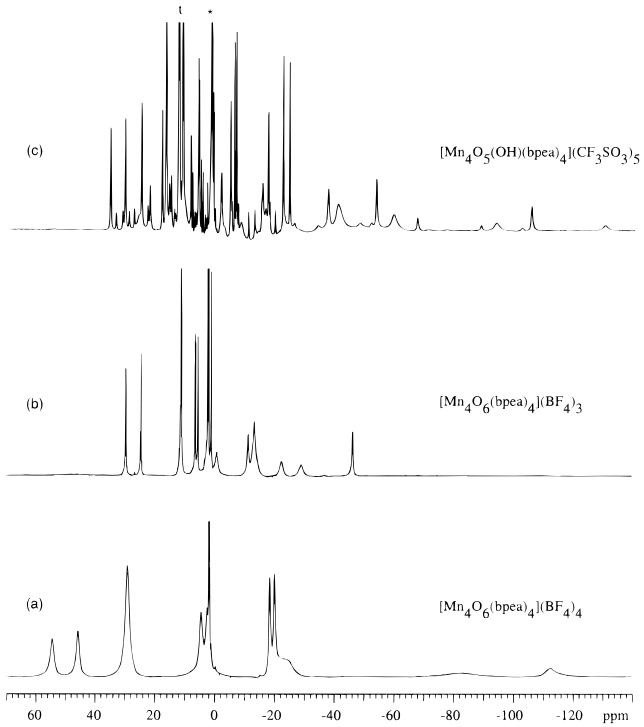

Figure 6. ^{1}H NMR spectra of (a) $[Mn_4O_6(bpea)_4](BF_4)_4$ (**1**$(BF_4)_4$), (b) $[Mn_4O_6(bpea)_4](BF_4)_3$ (**2**$(BF_4)_3$), synthesized by method B and recrystallized from CH_3CN/diethyl ether at −36 °C, and (c) $[Mn_4O_5(OH)(bpea)_4](CF_3SO_3)_5$ (**1**H$(CF_3SO_3)_5$), prepared by titration of **1**$(CF_3SO_3)_4$ with CF_3SO_3H (see Experimental Section for details). Conditions: CD_3CN, 299.95 MHz frequency, 295 K; *, CD_2HCN; t, CF_3SO_3H.

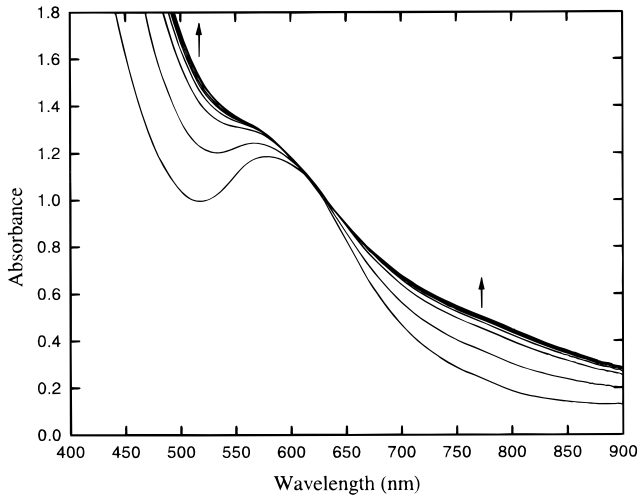

Figure 7. Spectrophotometric titration of $[Mn_4O_6(bpea)_4](CF_3SO_3)_4$ (**1**$(CF_3SO_3)_4$) in CH_3CN with CF_3SO_3H (isosbestic point at 625 nm). See Experimental Section for details.

consequently the protons on this ring experience a larger isotropic shift. Of the remaining ligand protons, four proton resonances are expected from bridging methylene groups, and two from the freely rotating ethyl moieties, giving rise to a total of 14 resonances in the ^{1}H NMR. In practice, there are seven broad resonances which are readily observable, and three even broader resonances which are typically more difficult to identify, spanning a 170 ppm spectral range, for compound **1** (for proton assignments see Table S_4 for **1**, **3**−**5**[91] and Table S5 for **2** and related complexes). The ^{1}H NMR signature of **2** (Figure 6b) is distinguished from that of **1** by a spectrum containing 14 sharper resonances spanning a narrower spectral range (71 ppm). The narrower spectral window and sharper resonances are consistent with the change from overall ferromagnetic to antiferromagnetic coupling.[23,92] Equivalence of the bpea ligands for **2** in solution indicates fast intramolecular electron transfer on the NMR time scale. On the other hand, the observation of distinct ^{1}H NMR spectra for **1** and **2**, as seen in the titration of **1** to **2** with Me_3-tacn (Figure S2), is a consequence of the slow rate of intermolecular electron transfer on the NMR time scale.[93]

Protonation Behavior. Structural and electronic changes concomitant with changes in the protonation state of the oxo-bridges have been observed for adamantane-like $\{Mn_4O_6\}^{4+}$ cores.[22,23] Unlike the aforementioned complexes, in which the oxo ligands are all equivalent, the lower symmetry of the bpea ligand creates site-differentiated oxo-bridges in **1** (vide supra). Furthermore, it seemed likely that the more sterically encumbered N-donor ligand bpea would enable us to regulate oxo-bridge acidity using both oxo group electron density and steric factors. We also felt that this much less basic N-donor ligand may provide an opportunity for promoting subsequent reactivity following protonation of an oxo-bridge.

Reversible protonation of an oxo-bridge of $[Mn_4O_6(bpea)_4](CF_3SO_3)_4$ in acetonitrile under argon with CF_3SO_3H to produce $[Mn_4O_5(OH)(bpea)_4](CF_3SO_3)_5$ (**1**H$^+$) (electrospray ionization mass spectrum of **1**H$^+$, Figure S9) was demonstrated spectrophotometrically (Figure 7) and by ^{1}H NMR (Figure 6c for **1** and Figure S10 for the bpma analog of **1**H$^+$, $[Mn_4O_5(OH)(bpma)_4]^{5+}$ (**3**H$^+$)). The observation of distinct ^{1}H NMR spectra for **1** and **1**H$^+$ for the titration of **1** with CF_3SO_3H is a consequence of the slow rate of proton self-exchange on the NMR time scale, and is consistent with data for other metal-oxo complexes.[23,94−97] Quantitative reversibility of protonation was verified by spectrophotometric back-titration with Et_3N. The effective pK_a of **1** of 1.54 ± 0.08 in acetonitrile[98,99] is, as expected for this ligand, the lowest pK_a value of the adamantane-like $\{Mn_4O_6\}^{4+}$ cores, which spans 11 orders of magnitude in acidity.[100]

The ^{1}H NMR spectrum of **1**H$^+$ (Figure 6c) reflects changes in core symmetry and magnetic properties of **1** following

(91) Wright, D. W.; Mok, H. J.; Dubé, C. E.; Armstrong, W. H. Manuscript in preparation.

(92) Bertini, I.; Luchinat, C. In *Physical Methods for Chemists*, 2nd ed.; Drago, R. S., Ed.; Saunders College Pub.: Fort Worth, 1992; pp 500−556.

(93) Rates of electron self-exchange for monomeric complexes in water range from 10^{-7} to 10^8 $M^{-1}s^{-1}$ (Marcus, R. A.; Sutin, N. *Biochim. Biophys. Acta* **1985**, *811*, 265−322).

(94) Kramarz, K. W.; Norton, J. R. In *Progress in Inorganic Chemistry*; Karlin, K. D., Ed.; Wiley: New York, 1994; Vol. 42, pp 1−65.

(95) Carroll, J. M.; Norton, J. R. *J. Am. Chem. Soc.* **1992**, *114*, 8744−8745.

(96) Fox, S.; Alaganandan, N.; Marten, W.; Karlin, K. D.; Blackburn, N. J. *J. Am. Chem. Soc.* **1996**, *118*, 24−34.

(97) Evans, D. R.; Mathur, R. S.; Heerwegh, K.; Reed, C. A.; Xie, Z. *Angew. Chem., Int. Ed. Engl.* **1997**, *36*, 1335−1337.

(98) pK_a values were calculated according to K_a(complex) = K_a(acid)/K_e, where K_e = [complex H$^+$][A$^-$]/[HA][complex]. K_e was determined using the change in absorbance at 750 and 515.9 nm. K_a(acid) values for the acids in CH_3CN are given by Izutsu (Izutsu, K. *Acid−Base Dissociation Constants in Dipolar Aprotic Solvents*; Blackwell Scientific Publications: Oxford, 1990; pp 17-35). The water content of UV−vis and ^{1}H NMR solutions was not measured, although CD_3CN showed no water by ^{1}H NMR. The water content of acetonitrile dried with 3 Å molecular sieves has been previously estimated to be 27 ppm (Burfield, D. R.; Lee, K.-H.; Smithers, R. M. *J. Org. Chem.* **1977**, *42*, 3060−3065). Water (pK_a in acetonitrile = 2.4) will be a competitive base with a weak base such as **1**, and will result in an effective pK_a value which is lower than the absolute value.

(99) An aqueous pK_a for **1**$(CF_3SO_3)_4$ of −6.0 is estimated from the relation p$K_a(H_2O)$ = p$K_a(CH_3CN)$−7.5 (Kristjansdottir, S. S.; Norton, J. R. In *Transition Metal Hydrides*; Dedieu, A., Ed.; VCH Publishers: New York, 1992; pp 309−359).

protonation. A μ_{eff}/Mn of 3.42 μ_B for $\mathbf{1}H^+$ compares with 4.65 μ_B for **1**, and reflects a change from overall ferromagnetic to overall moderately antiferromagnetic coupling, similar to the change in magnetic moment seen for the protonation of the other adamantane-shaped $\{Mn_4O_6\}^{4+}$ cores.[22,23] The change in magnetic coupling of $\mathbf{1}H^+$ is readily observed in its ^{1}H NMR spectrum, which is characterized by proton resonances with much narrower line widths than those of **1**.

The ^{1}H NMR spectrum of $\mathbf{1}H^+$ also highlights the change in symmetry of the core with protonation. Given that the S_4 symmetry of **1** results in two inequivalent oxo-bridges (type A and type B), there arises the possibility for two protonation isomers. Protonation at site B (protonation isomer B) results in two inequivalent bpea ligands, and protonation at site A (protonation isomer A) renders all four of the bpea ligands inequivalent, for a total of 84 possible resonances in the ^{1}H NMR spectrum of $\mathbf{1}H^+$. In fact, both protonation isomers are observed (*vide infra*), although only 65 of the 84 predicted resonances are readily detected, spanning a spectral window from −102 to 38 ppm (Figure 6c). The ^{1}H NMR analysis is somewhat simplified if $\mathbf{3}H^+$ is used (Figure S10). The elimination of six methylene resonances reduces the total number of expected resonances to 78, of which 67 are observed (Table S6 histogram of data in Figure S11). Based on the assignment of the ^{1}H NMR resonances for the 3, 4, and 5 pyridyl ring positions of **1** and **3** (Table S4) along with the aid of the methyl-substituted analogs of $\mathbf{3}H^+$, $\mathbf{4}H^+$and $\mathbf{5}H^+$, the 4 and 5 position ring protons (and by the process of elimination the 3 position ring protons) are readily identifiable as groups of four resonances of equal intensity for isomer B (Table S10). Similarly, these same protons are identifiable as groups of eight resonances of equal intensity for isomer A. Location of the methylene protons of $\mathbf{1}H^+$ and $\mathbf{3}H^+$ in ^{1}H NMR spectra is aided by comparison with the ^{1}H NMR spectrum of $[Mn_4O_5(OH)(tacn)_4]^{5+}$ ($\mathbf{6}H^+$),[23] the methylene proton resonances of which are in the range $-20 < \delta < -120$ ppm.

Based on crystallographic analysis of **1**, we expected that the type A oxo-bridges (average Mn−O_{oxo} bond length 1.806 Å) would be more acidic than the shorter type B oxo-bridges (average bond length 1.786 Å). However, there are twice as many A sites as B sites, giving a statistical contribution to ΔpK_a between the two sites of 0.3 units. Furthermore, the crystal structure of **1** suggests that the A site could be more sterically hindered, increasing its acidity. The net effect of these factors, as measured by a comparison of integrals of the 4 and 5 ring protons of each isomer (Table S6), indicates that a solution of $\mathbf{1}H^+$, as well as $\mathbf{3}H^+$, consists of 24% A and 76% B. Given that isomers A and B are in equilibrium, it was possible to determine that the effective pK_a of site A (0.91) is measurably lower than that of site B (1.42),[102] despite an entropic contribution of 0.3 pK_a units for site A. These data also suggest that no further steric hindrance to protonation of the oxo-bridges was encountered in going from methyl to ethyl groups on the N_{alkyl} atom. We are currently investigating the effect of bulkier N_{alkyl} atom substituents on oxo-bridge protonation.

The similarities and differences in solution structure of the one-electron reduced complex **2** and the monoprotonated complex $\mathbf{1}H^+$ require comment. Although both $\mathbf{1}H^+$ and **2** have overall antiferromagnetic coupling of similar magnitude, the differences in the effective solution electronic structure, as determined by ^{1}H NMR, derive in large part from the difference in rate of intramolecular exchange of electrons (fast) and protons (slow) for **2** and **1**, respectively, on the NMR time scale. Time-averaged equivalence of the Mn ions for **2** gives rise to solution structural symmetry similar to that found in **1**, hence a ^{1}H NMR spectrum (Figure 6b) similar to that of **1** (Figure 6a), with sharper resonances and a narrower spectral window to reflect the overall antiferromagnetic coupling. Proton exchange for $\mathbf{1}H^+$ is slow in solution on the NMR time scale, however, and consequently two (isomer B) or all four (isomer A) of the Mn ions of $\mathbf{1}H^+$are inequivalent. A μ_{eff}/Mn of 3.42 μ_B for $\mathbf{1}H^+$ is a composite of the two isomers, however, a comparison of similar proton resonances for each species shows that the isomers have similar spectral windows, suggesting that the isomers have comparable overall effective magnetic moments. The greater overall breadth of the ^{1}H NMR spectrum of $\mathbf{1}H^+$ compared with that of **2** in large part can be attributed to differences in local magnetic moments of the individual Mn^{IV} ions of $\mathbf{1}H^+$.

Having demonstrated both reversible reduction and protonation of **1**, we subsequently demonstrated that reduction of the $[Mn_4O_6(bpea)_4]^{4+}$ core in H_2O could also be coupled to proton transfer, a phenomenon not observed for the tacn and tame analogs.

Proton-Coupled Electron Transfer. In aqueous solution (pH 7), complex **1** demonstrated a well-behaved quasi-reversible wave at +0.06 V, ΔE_p = 135 mV, (500 mVs^{-1} scan rate)[103] using a Pt button or glassy carbon electrode (Figure 8). The pH dependence of the electrochemical behavior of **1** in aqueous phosphate buffer (0.1 M) is shown in Figure 9 for the pH range 1.05−11.04. Between pH 11.04 and 3.51, the slope of the biphasic Pourbaix diagram is 44 mV/pH unit. Although this is somewhat lower than the predicted value of 59 mV/pH unit required for a one-electron, one-proton couple, we assign this wave to the process:

$$[Mn_4O_6(bpea)_4]^{4+} + H^+ + e^- \rightleftharpoons [Mn_4O_5OH(bpea)_4]^{4+} \quad (2)$$

In the pH range 3.51−1.05, the slope of the Pourbaix diagram is 115 mV/pH unit. Such a slope is consistent with a one-electron, two-proton couple such as

$$[Mn_4O_6(bpea)_4]^{4+} + 2H^+ + e^- \rightleftharpoons [Mn_4O_4(OH)_2(bpea)_4]^{5+} \quad (3)$$

which would have a predicted slope of 118 mV/pH unit.

The unique aqueous proton-coupled electron-transfer behavior of **1** is significantly different from that observed in other manganese-oxo aggregates. Previously, only single proton-coupled electron transfer has been ascribed to manganese-oxo dimers such as $[Mn_2O_2(bpy)_4]^{3+}$ and $[Mn_2O_2(edda)_2]^-$.[105] The dimeric $[Mn_2O_2(phen)_4]^{3+}$ complex displays two separate one-

(100) The highest pK_a among the $\{Mn_4O_6\}^{4+}$ cores of 12.5, for the first protonation of $[Mn_4O_6(tame)_4](CF_3SO_3)_4$, was determined by spectrophotometric titration with pyridinium triflate in acetonitrile (Dubé, C. E.; Armstrong, W. H. Unpublished work).

(101) The magnetic susceptibility characteristics of $\mathbf{1}H^+$ in solution at 295 K were determined by the NMR method. See Experimental Section for preparation of samples of $\mathbf{1}H^+$.

(102) K_a of isomer B is determined from the relation $K_a^{obs} = K_eK_a(B)/(1 + K_e)$, where K_a^{obs} is the measured K_a of the mixture of isomers and K_e is the equilibrium constant relating the two isomers. The pK_a of isomer A is given by pK_a (A) = pK_a(B) − log K_e.

(103) The protonated/reduced complexes $\mathbf{2}H^+$ and $\mathbf{2}(H^+)_2$ exhibited degradation in aqueous solution by cyclic voltammetry at slower scan rates. Reproducible voltammograms of the coupled processes were collected at 500 mV/s. Voltammetry of aqueous solutions of **1** above pH about 12 was not possible because of complex degradation.

(104) Thorp, H. H.; Sarneski, J. E.; Brudvig, G. W.; Crabtree, R. H. *J. Am. Chem. Soc.* **1989**, *111*, 9249−9250.

(105) Manchanda, R.; Thorp, H. H.; Brudvig, G. W.; Crabtree, R. H. *Inorg. Chem.* **1991**, *30*, 494−497.

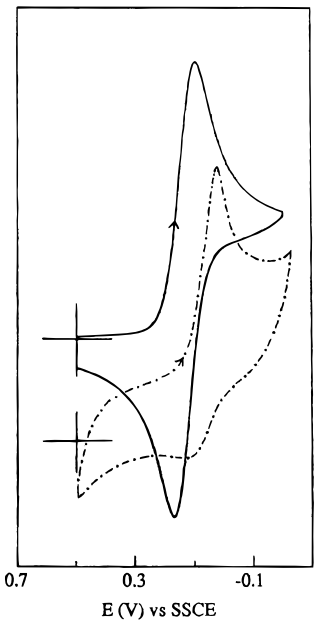

Figure 8. Cyclic voltammograms of the quasi-reversible redox couple of $[Mn_4O_6(bpea)_4](ClO_4)_4$ (**1**$(ClO_4)_4$) (0.81 mM) in 0.2 M TBAP in acetonitrile (scan rate of 50 mV/s) (—) and $[Mn_4O_6(bpea)_4](SCN)_4 \cdot 3H_2O$ (**1**$(SCN)_4 \cdot 3H_2O$) (0.68 mM) in 0.1 M aqueous phosphate buffer (pH 7) (scan rate 500 mV/s) (—·—). See Experimental Section for details.

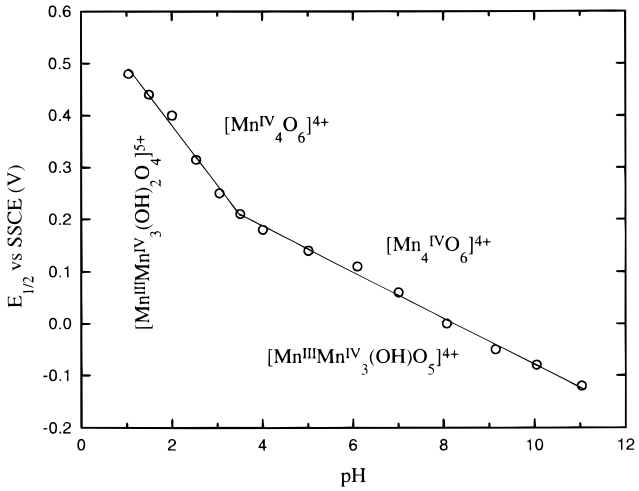

Figure 9. Pourbaix diagram detailing the pH dependence of the electrochemical behavior of $[Mn_4O_6(bpea)_4](SCN)_4 \cdot 3H_2O$ (**1**$(SCN)_4 \cdot 3H_2O$) in 0.1 M aqueous phosphate buffer. The data were obtained at a scan rate of 500 mV/s with a Pt button working electrode and potentials are reported versus SSCE. See text for analysis and discussion of the proton-coupled electron-transfer behavior of **1**.

proton, one-electron coupled transfer events for the III,IV/III,-III couple of $[Mn_2O_2(phen)_4]^{3+}$ and the III,III/III,II couple of $[Mn_2O(OH)(phen)_4]^{2+}$, respectively.[106] In contrast to these well-behaved systems, the related dimer $[Mn_2O_2(bispicen)_3]^{3+}$ demonstrates an uncoupled one-electron reduction followed by rapid protonation of the bridging oxo group.[105] Recently, proton-coupled electron transfer has also been described for the Mn-(IV,IV) complex $[Mn_2O_3(Me_3tacn)_2]^{2+}$ in which the complex demonstrates a pH-independent region at pH values greater than 4 and a pH-dependent region between pH 1 and 4.[107] Although the biphasic multiple-proton-coupled electron-transfer behavior of **1** has been previously unobserved for manganese-oxo complexes, such behavior has been noted for $[(trpy)(bpy)Ru^{IV}O]^{2+}$ and $[(trpy)(bpy)Os^{IV}O]^{2+}$,[108] and in the oxidative direction for $[Ru_2O(bpy)_4(H_2O)_2]^{4+}$.[109]

From the Pourbaix diagram, it is possible to estimate the successive pK_a values of the one-electron reduced species. Given that well-behaved proton-coupled electron transfer is observed for **1** up through pH 11, and that the electrochemical behavior of the complex at pH 12 suggests degradation, it is possible to place a lower limit of the pK_a for $[Mn^{IV}_3Mn^{III}O_6(bpea)_4]^{3+}$ near 11.5.[110] A more exact value for the pK_a of $[Mn^{IV}_3Mn^{III}O_5(OH)(bpea)_4]^{4+}$ can be determined from the inflection point in the Pourbaix diagram at pH 3.51. This decrease in the pK_a value by at least 8 orders of magnitude following protonation is similar to that observed in the successive protonation of the Mn(IV) adamantane-shaped $[Mn_4O_6(tacn)_4]^{4+}$, and it is significantly larger than the 3−5 unit change observed for successive protonation of $[Mn(X\text{-salpn})(\mu\text{-}O)]_2$.[111] In addition, these electrochemical studies highlight the remarkable change in the core's basicity upon reduction. Given the pK_a estimate of −6.0 for $[Mn_4O_6(bpea)_4]^{4+}$, and the estimate of 11.5 for $[Mn^{IV}_3Mn^{III}O_6(bpea)_4]^{3+}$ (a lower limit), a one-electron reduction of the core results in an effective increase in the basicity of the oxo-bridges by at least 17.5 orders of magnitude. This is twice the change in basicity observed for $[Mn_2O_2(bpy)_4]^{3+}$ upon reduction.[104] Recently, Baldwin and Pecoraro[112] mimicked the net result of a proton-coupled electron-transfer event using the $[Mn(X\text{-salpn})(\mu\text{-}O)]_2$ model system for X = H, 3,5-$(Cl)_2$, and 3,5-$(NO_2)_2$, in which the basicity of the oxo-bridges increased by 11.1−8.3 orders of magnitude upon reduction.

Several mechanistic arguments have been proposed to explain the observed pH-mediated electrochemistry of manganese-oxo complexes. For example, to explain the proton-coupled electron transfer of $[Mn_2O_2(bpy)_4]^{3+}$ versus the sequential reduction/protonation of $[Mn_2O_2(bispicen)_3]^{3+}$, it was proposed that the methylene groups of the bispicen ligand provided a steric hindrance to the oxo-bridges, thereby uncoupling the protonation step from the reduction.[105,113] The crystal structure of **1** clearly reveals a core more sterically hindered than that of the bispicen complex,[114] yet **1** undergoes proton-coupled electron transfer. Alternatively, it has been suggested that the decoupled electron transfer in $[Mn_2O_2(bispicen)_2]^{3+}$ is because the basicity of the oxo-bridges is insufficient for them to be protonated.[105,113] However, the pK_a value of $[Mn_4O_6(bpea)_4]^{4+}$ is almost 6 orders

(106) Manchanda, R.; Thorp, H. H.; Brudvig, G. W.; Crabtree, R. H. *Inorg. Chem.* **1992**, *31*, 4040−4041.

(107) Hage, R.; Krijnen, B.; Warnaar, J. B.; Hartl, F.; Stufkens, D. J.; Snoeck, T. L. *Inorg. Chem.* **1995**, *34*, 4973−4978.

(108) Takeuchi, K. J.; Thompson, M. S.; Pipes, D. W.; Meyer, T. J. *Inorg. Chem.* **1984**, *23*, 1845−1851.

(109) Gilbert, J. A.; Eggleston, D. S.; Murphy, W. R., Jr.; Geselowtiz, D. A.; Gersten, S. W.; Hodgson, D. J.; Meyer, T. J. *J. Am. Chem. Soc.* **1985**, *107*, 3855−3864.

(110) Attempts to determine the pK_a of **2** directly by titration with acid in acetonitrile were unsuccessful owing to conversion of **2** to **1** at about 75% yield based on spectrophotometrically monitored reactions. An approximate pK_a for **2** of 20 in acetonitrile was determined using weak acids with pK_a values ranging from 19 to 23. The approximate pK_a in water is 13 (vide supra). The conversion of **2** to **1** with protonation is under investigation.

(111) Baldwin, M. J.; Stemmler, T. L.; Riggs-Gelasco, P. J.; Kirk, M. L.; Penner-Hahn, J. E.; Pecoraro, V. L. *J. Am. Chem. Soc.* **1994**, *116*, 11349−11356.

(112) Baldwin, M. J.; Pecoraro, V. L. *J. Am. Chem. Soc.* **1996**, *118*, 11325−11326.

(113) See ref 75.

(114) Collins, M. A.; Hodgson, D. J.; Michelsen, K.; Towle, D. K. *J. Chem. Soc., Chem. Commun.* **1987**, 1659−1660.

of magnitude lower than that estimated for $[Mn_2O_2(bispicen)_2]^{3+}$, yet readily undergoes proton-coupled electron transfer. It is also noteworthy in the present investigation that unlike the pH-dependent electrochemistry of $[Mn_2O_2(bpy)_4]^{3+}$, which is very much influenced by the nature of the electrode surface,[116] the proton-coupled electron transfer for **1** was similar for both glassy carbon and bare Pt metal electrodes. It is evident from this limited set of examples that the mechanistic origin of proton-coupled electron transfer for manganese-oxo complexes is poorly understood, and that factors such as steric hindrance of the oxo-bridges, the pK_a value of these bridges, or the nature of the electrode surface alone are not sufficient to predict whether a system will undergo sequential or coupled electron/proton-transfer chemistry.

Concluding Remarks

Although the EXAFS analysis of the Mn-oxo core within PSII suggests that the adamantane-shaped $\{Mn_4O_6\}^{4+}$ core is too symmetrical and the Mn···Mn distance is too long to be considered as an accurate *structural* model of the S_0-S_2 states of the active site,[88] we have shown that the tetranuclear aggregate **1** undergoes a variety of reactivities which have *mechanistic* implications with regard to substrate oxidation at the active site. For instance, many of the mechanisms proposed for water oxidation invoke formation of a manganese-peroxo species by O−O bond formation prior to release of O_2.[34,36,117,118] In the event that bridging oxo ligands gives rise to a peroxo species, oxygen atoms poised for O−O bond formation in the water oxidase active site have a lower electron density than that of two O^{2-} ions. As a consequence of this model, activating O^{2-} for O−O bond formation by reducing oxo ligand electron density is a primary goal in the synthesis of high valent manganese-oxo clusters. The donor properties of the ancillary ligands of these complexes play an important role in tuning the oxo-bridge electron density of the manganese-oxo cores. In this regard the bpea ligand in **1** is used to stabilize the most "activated" bridging oxo ligands of all dinuclear and tetranuclear Mn^{IV}-oxo complexes for which oxo-bridge pK_a data are available, and this could conceivably facilitate formation of an O−O bond between two adjacent oxo ligands.

Another interesting property of **1** is the subsite differentiation of the oxo-bridges by virtue of the steric and electronic properties of the ligand. In a number of metalloproteins the metals composing the active site cluster are differentiated by a combination of amino acid ligation, steric interactions between the metal cluster and amino acid residues, and hydrogen bonding. It is, therefore, reasonable to postulate that the Mn-oxo core of the OEC may be influenced to some extent by modest differences in active site amino acid residues. Such factors are, however, difficult to incorporate into structural models of metalloproteins due to the symmetric nature of many common ligands in the spontaneous self-assembly approach used to target relatively simple cluster topologies. Some Mn-oxo dimeric systems have achieved oxo-bridge discrimination by the asymmetric coordination of different ligands to the metal ions, as demonstrated in the solid-state structure of the asymmetric $[Mn_2O_2(OAc)(Me_3tacn)(\eta_2\text{-}OAc)(\eta_1\text{-}OAc)]^+$ complex.[119] In contrast, the differentiation of oxo-bridges in **1** is accomplished by more subtle means. X-ray crystallographic analysis and ^{1}H NMR protonation studies of **1** reveal that the interplay of electronic and steric properties of the bpea ligand in the adamantane-shaped $\{Mn_4O_6\}^{4+}$ core generates two chemically distinct oxo sites. The differentiated sites within complex **1** demonstrate how amino acid side chains might similarly differentiate the site of substrate binding within the Mn complex of the OEC.

In intact preparations of PSII, an extrinsic pattern of proton release coupled to S state advancement has been observed. Measurements of the extrinsic proton release have been interpreted as a stoichiometry of 1:0:1:2 for the $S_0 \rightarrow S_1$, $S_1 \rightarrow S_2$, $S_2 \rightarrow S_3$, $S_3 \rightarrow (S_4) \rightarrow S_0$ transitions, respectively.[120] Other measurements suggest a pH-dependent noninteger stoichiometry.[121,122] For example, for the same sequence of oxidation steps a 1.2:0.2:0.95:1.65 stoichiometry was determined at a pH of 6.5.[122] The proton-coupled electron-transfer behavior of **1** is significant among reported Mn-oxo model systems of the water oxidizing complex because it is the first example of a Mn-oxo aggregate exhibiting a $e^-/2H^+$ stoichiometry and because it diaplays a pH-dependent e^-/H^+ stoichiometry. It is likely that access to both e^-/H^+ and $e^-/2H^+$ stoichiometries is potentiated by the dramatic shift in basicity of the $\{Mn_4O_6\}$ core attendant with the change in oxidation state. The pH-mediated electrochemistry of **1** underlies the potential importance of the effective pH in the immediate vicinity of the water oxidizing complex, and reflects the importance of prior deprotonation events within the S cycle, most notably from the specific histidine or tyrosine involved in the S-state transitions.[123−125]

Acknowledgment. We thank Dr. John G. Boylan for helpful suggestions on design and analysis of ^{1}H NMR experiments and Henry J. Mok for help with the ligand synthesis. Funding for this research was provided by National Institutes of Health grant GM38275. The National Institutes of Health grant 1 S10 RR09008 and Boston College provided funds for purchase of a Siemens SMART single crystal X-ray diffractometer and the W. M. Keck Foundation provided funds for the SQUID magnetometer at Tufts University.

Supporting Information Available: Supporting Information Available: A description of the synthesis of **3**$(ClO_4)_4$, **4**$(ClO_4)_4$, and **5**$(ClO_4)_4$; a plot of bulk coulometry charge versus time (Figure S1); ^{1}H NMR stack plot of titration of **1** with Me_3-tacn to **2** (Figure S2); complete ORTEP plots of **1** (Figure S3) and **2** (Figure S4); electrospray mass spectra of **1** (Figure S5), **2** (Figure S6), and **6** (Figure S7); μ_{eff} vs temperature of **1** (Figure S8); electrospray mass spectrum of **1**H$(CF_3SO_3)_5$ (Figure S9);

(115) A pK_a of approximately 0 is estimated for $[Mn_2O_2(bispicen)_2]^{3+}$ based on a comparison of the pK_a value of $[Mn_2O_2(bispicen)_2]^{2+}$ (8.3) with pK_a values of $[Mn_2O_2(bpy)_4]^{3+}$ and $[Mn_2O_2(bpy)_4]^{2+}$ (11.0 and 2.3, respectively (Thorp, H. H.; Sarneski, J. E.; Brudvig, G. W.; Crabtree, R. H. *J. Am. Chem. Soc.* **1989**, *111*, 9249−9250)), and a pK_a of 9.2 for $[Mn_2O_2(phen)_4]^{2+}$ (Manchanda, R.; Thorp, H. H.; Brudvig, G. W.; Crabtree, R. H. *Inorg. Chem.* **1992**, *31*, 4040−4041).

(116) Thorp, H. H.; Brudvig, G. W.; Bowden, E. F. *J. Electroanal. Chem. Interfacial Electrochem.* **1990**, *290*, 293−301.

(117) Armstrong, W. H. In *Manganese Redox Enzymes*; Pecoraro, V. L., Ed.; VCH Publishers: New York, 1992; pp 261−286.

(118) Proserpio, D. M.; Rappé, A. K.; Gorun, S. M. *Inorg. Chim. Acta* **1993**, *213*, 319−324.

(119) Bossek, U.; Saher, M.; Weyhermuller, T.; Wieghardt, K. *J. Chem. Soc., Chem. Commun.* **1992**, 1780−1782.

(120) Forster, V.; Hong, Y. Q.; Junge, W. *Biochim. Biophys. Acta* **1981**, *638*, 141−152.

(121) Jahns, P.; Lavergne, J.; Rappaport, F.; Junge, W. *Biochim. Biophys. Acta* **1991**, *1057*, 313−319.

(122) Rappaport, F.; Lavergne, J. *Biochemistry* **1991**, *30*, 10004−10012.

(123) Tommos, C.; Tang, X.-S.; Warncke, K.; Hoganson, C. W.; Styring, S.; McCracken, J.; Diner, B. A.; Babcock, G. T. *J. Am. Chem. Soc.* **1995**, *117*, 10325−10335.

(124) Gilchrist, M. L., Jr.; Ball, J. A.; Randall, D. W.; Britt, R. D. *Proc. Natl. Acad. Sci. U.S.A.* **1995**, *92*, 9545−9549.

(125) Tang, X.-S.; Randall, D. W.; Force, D. A.; Diner, B. A.; Britt, R. D. *J. Am. Chem. Soc.* **1996**, *118*, 7638−7639.

^{1}H NMR stack plot of titration of **3** with CF_3SO_3H (Figure S10), bar graph of ^{1}H NMR peak intensities for **3**H$(CF_3SO_3)_5$ (Figure S11); tables of metathesis yield, elemental analysis, and characterization of **1**X_4 (X = Br^-, BF_4^-, $CF_3SO_3^-$, PF_6^-, SCN^-, and BAr'_4^-) (Table S1) and **3**$(ClO_4)_4$, **4**$(ClO_4)_4$, and **5**$(ClO_4)_4$ (Table S2); selected structural and vibrational data of adamantane-like aggregates (Table S3); ^{1}H NMR data for **1**, **3**, **4**, **5** (Table S4), **2** (and related complexes) (Table S5), and **3**H$(CF_3SO_3)_5$ (Table S6); full crystallographic information, atomic coordinates, and U_{eq}; intramolecular bond distances and angles, anisotropic displacement parameters, hydrogen coordinates; and isotropic displacement parameters for **1** and **2** (Tables S7-S16) (52 pages). See any current masthead page for ordering and Web access instructions.

JA973668V